

The rapid transition from shallow to precipitating convection as a predator-prey process

Cristian Valer Vraciu¹, Julien Savre², and Maxime Colin³

¹Horia Hulubei National Institute of Physics and Nuclear Engineering

²Ludwig-Maximilians-University

³Leibniz Centre for Tropical Marine Research

March 05, 2024

Abstract

Properly predicting the rapid transition from shallow to precipitating atmospheric convection within a diurnal cycle over land is of great importance for both weather prediction and climate projections. In this work, we consider that a cumulus cloud is formed due to the transport of water mass by multiple updrafts during its life-time. Cumulus clouds then locally create favorable conditions for the subsequent convective updrafts to reach higher altitudes, leading to deeper precipitating convection. This mechanism is amplified by the cold pools formed by the evaporation of precipitation in the sub-cloud layer. Based on this conceptual view of cloud-cloud interactions which goes beyond the one cloud equals one-plume picture, it is argued that precipitating clouds may act as predators that prey on the total cloud population, such that the rapid shallow-to-deep transition can be modeled as a simple predator-prey system. This conceptual model is validated by comparing solutions of the Lotka-Volterra system of equations to results obtained using a high-resolution large-eddy simulation model. Moreover, we argue that the complete diurnal cycle of deep convection can be seen as a predator-prey system with varying food supply for the prey. Finally, we suggest that the present model can be applied to weather and climate models, which may lead to improved representations of the transition from shallow to precipitating continental convection.

The rapid transition from shallow to precipitating convection as a predator–prey process

Cristian V. Vraciu^{1,2}, Julien Savre³, Maxime Colin⁴

¹Faculty of Physics, University of Bucharest, Bucharest–Măgurele, Romania

²Department of Theoretical Physics, Horia Hulubei National Institute of Physics and Nuclear Engineering, Măgurele, Romania

³Meteorology Institute, Ludwig-Maximilians-Universität München, Munich, Germany

⁴Leibniz Centre for Tropical Marine Research, Bremen, Germany

Key Points:

- A conceptual picture for cumulus cloud populations based on cloud–updraft interaction is discussed
- The local shallow preconditioning and the cold pool feedback imply a predator–prey type of interaction in the cloud–precipitation system
- A simple predator–prey model shows good agreement with idealized numerical simulations for the rapid shallow–to–deep transition.

Corresponding author: Cristian V. Vraciu, cristian.vraciu@theory.nipne.ro

16 Abstract

17 Properly predicting the rapid transition from shallow to precipitating atmospheric con-
 18 vection within a diurnal cycle over land is of great importance for both weather predic-
 19 tion and climate projections. In this work, we consider that a cumulus cloud is formed
 20 due to the transport of water mass by multiple updrafts during its life-time. Cumulus
 21 clouds then locally create favorable conditions for the subsequent convective updrafts
 22 to reach higher altitudes, leading to deeper precipitating convection. This mechanism
 23 is amplified by the cold pools formed by the evaporation of precipitation in the sub-cloud
 24 layer. Based on this conceptual view of cloud-cloud interactions which goes beyond the
 25 one cloud equals one-plume picture, it is argued that precipitating clouds may act as preda-
 26 tors that prey on the total cloud population, such that the rapid shallow-to-deep tran-
 27 sition can be modeled as a simple predator-prey system. This conceptual model is val-
 28 idated by comparing solutions of the Lotka-Volterra system of equations to results ob-
 29 tained using a high-resolution large-eddy Simulation model. Moreover, we argue that the
 30 complete diurnal cycle of deep convection can be seen as a predator-prey system with
 31 varying food supply for the prey. Finally, we suggest that the present model can be ap-
 32 plied to weather and climate models, which may lead to improved representations of the
 33 transition from shallow to precipitating continental convection.

34 Plain Language Summary

35 The rapid transition from shallow to precipitating convection over land is still poorly rep-
 36 resented by weather and climate models. In this work, we argue that this is due to the
 37 fact that the convective parameterization schemes only consider the interaction between
 38 the clouds and their environment, which is a slow process, and do not consider cloud-
 39 cloud interactions during the transition, which is a fast process. We show that this lat-
 40 ter interaction can be modeled as a predator-prey process, and we show how a very sim-
 41 ple dynamical model for cloud population can lead to improved prediction for the pre-
 42 cipitation rate and cloud cover over land.

43 1 Introduction

44 Atmospheric convection transports heat and moisture from the surface throughout the
 45 troposphere creating cumulus and cumulonimbus clouds that are responsible for the wa-
 46 ter cycle in the atmosphere and have a strong radiative forcing that can lead to either
 47 warming or cooling of the atmosphere. Shallow cumulus clouds are non-precipitating,
 48 or weakly precipitating convective clouds that form when the updraft plumes from the
 49 boundary layer reach the lifting condensation level but are unable to reach higher alti-
 50 tudes as they lose their buoyancy very quickly. Predicting shallow clouds is very impor-
 51 tant for climate predictability as they cover a very large part of the Earth and have a
 52 strong cooling effect on the climate system since they reflect an important fraction of
 53 the solar radiation back into space. When the atmosphere is unstable and the updraft
 54 plumes are able to reach the level of free convection, deep, precipitating convection is
 55 initiated. The deep convective clouds (congestus and cumulonimbus) precipitate, and
 56 re-stabilize the atmosphere as they warm and dry their environment. Since the cumu-
 57 lonimbus clouds are responsible for the formation of cirrus clouds, they also play a very
 58 important role in controlling the radiative budget of the Earth, as the cirrus clouds have
 59 a net warming effect. Therefore, the manner shallow and deep convective clouds are rep-
 60 resented in climate models has a significant impact on climate predictions.

61 In general, the presence of a convective inhibition (CIN) layer prevents boundary
 62 layer updrafts from spontaneously reaching their level of free convection and slows down
 63 the development of deep precipitating clouds: in this situation, shallow cumuli develop
 64 first and contribute to the creation of conditions favorable to deep convection. The tran-

65 sition from shallow to precipitating convection can be considered of two types: (i) a slow
66 transition when at the beginning the atmosphere is not unstable enough to sustain the
67 development of precipitating convection, and the shallow cumuli slowly moisten the at-
68 mosphere until the environment is unstable enough to allow the clouds to grow deeper
69 and precipitate (Yano & Plant, 2012b; Champouillon et al., 2023), which is a process that
70 takes typically a few days; (ii) a rapid transition in which the atmosphere is already un-
71 stable but deep precipitating convection still takes a few hours to develop. This rapid
72 transition occurs usually over the tropics where the atmosphere is always unstable (Hohenegger
73 & Stevens, 2013). In a diurnal cycle over land, the rapid transition has been documented
74 by several authors (Grabowski et al., 2006; Khairoutdinov & Randall, 2006; Kurowski
75 et al., 2018; Grabowski, 2023; Savre & Craig, 2023). In this particular case, the tran-
76 sition starts when the convective inhibition becomes small, and it takes around 3-4 hours
77 for precipitation to properly develop, despite having a very large convective available po-
78 tential energy (CAPE) from the beginning. In this study, we focus on the second kind
79 of shallow-to-deep transition.

80 Although in recent years many studies investigated the physical processes control-
81 ling the rapid transition from shallow to precipitating convection (Kurowski et al., 2018;
82 Peters et al., 2022; Powell, 2022; Rochetin et al., 2014; Schiro & Neelin, 2019), weather
83 and climate models still predict the onset of deep precipitating convection to occur around
84 2-5 hours earlier when compared to observations (Christopoulos & Schneider, 2021) or
85 large-eddy simulation (LES) (Bechtold et al., 2004; Grabowski et al., 2006; Couvreux
86 et al., 2015; Harvey et al., 2022; Tao et al., 2023) within a diurnal cycle over land. That
87 is because the convective parameterization schemes immediately switch to deep convec-
88 tion when CIN is very small and CAPE is large, although in reality, even when these con-
89 ditions are met, the transition still takes a few hours, or may not even occur within a
90 diurnal cycle (Khairoutdinov & Randall, 2006; Nelson et al., 2021; Tian et al., 2021; Zhuang
91 et al., 2017).

92 The majority of convective parameterization schemes used in climate models are
93 based on the so-called mass-flux parameterization. The objective of these parameter-
94 izations is to find the mass flux of the clouds and to provide feedback to the large-scale
95 resolved by the model. The mass-flux formulation is based on the idea that the clouds,
96 or the whole ensemble of clouds, can be modeled as steady-state plumes. In the picture
97 used by these formulations, a convective cloud is formed by only one entraining plume,
98 which only entrains environmental air described by the mean resolved state (Arakawa,
99 2004; Plant, 2010; Yano, 2014). Thus, the mass flux is estimated in these parameteri-
100 zation schemes only by considering the large-scale state, neglecting any cloud-cloud in-
101 teraction or heterogeneity within a given grid box. As the mass flux only changes with
102 the slow change of the large-scale state, these schemes are unable to catch any rapid tran-
103 sition from shallow to precipitating convection (Bechtold et al., 2004). At the time Arakawa
104 and Schubert (1974) formulated their parameterization, the grid box and the time-stepping
105 used by climate models were so large that over the tropical ocean one could consider that
106 at all times within a grid-box there is a spectrum of shallow and precipitating clouds
107 that are in quasi-equilibrium with their environment. Many operational parameteriza-
108 tion schemes still follow the original mass-flux formulation introduced by Arakawa and
109 Schubert (1974) (e.g., Bechtold et al., 2014; Kain & Fritsch, 1993; Rio et al., 2019). How-
110 ever, nowadays, climate models have much finer resolutions, both in space and time, and
111 the quasi-equilibrium is therefore not satisfied in every grid box at every time step (Davies
112 et al., 2013; Donner & Phillips, 2003; Jones & Randall, 2011). To improve the represen-
113 tation of atmospheric convection in numerical models with high temporal resolution, sev-
114 eral prognostic closures for the convective mass flux with relaxed quasi-equilibrium have
115 later been formulated (e.g., Moorthi & Suarez, 1992; Pan & Randall, 1998; Wagner &
116 Graf, 2010; Yano & Plant, 2012a)

117 In general, the time evolution of the convective mass flux at cloud base M_c can be
 118 written as:

$$\frac{dM_c}{dt} = \rho_0 \sigma_c \frac{dw_c}{dt} + \rho_0 w_c \frac{d\sigma_c}{dt}, \quad (1)$$

119 where t is the time, ρ_0 is the atmospheric density at the cloud base, σ_c is the convective
 120 cloud cover, and w_c is the convective updraft velocity of the convective clouds. The mass-
 121 flux parameterizations usually consider that σ_c is constant, and thus, only the first term
 122 on the right hand side (rhs) of Equation 1 is important. Although the traditional mass-
 123 flux formulations do not make the assumption that σ_c is constant in an explicit way, such
 124 an assumption can be easily justified if the grid box and the time step are very large,
 125 such that the fluctuations in σ_c are subgrid, and the increase in cloud population in a
 126 small subdomain is compensated by the decay of clouds in another small subdomain. There-
 127 fore, in the mass-flux parameterization schemes, the triggering of individual convective
 128 clouds is not considered, but rather the whole spectrum of clouds that slowly interacts
 129 with the large-scale environment (Yano et al., 2013). It should also be noted that pa-
 130 rameterization models that implement a momentum equation for w_c have been formu-
 131 lated (e.g., Donner, 1993; Bechtold et al., 2001; Bretherton et al., 2004), in which the
 132 assumption that σ_c is constant is made in an explicit way. As in the original mass-flux
 133 formulation based on quasi-equilibrium, the prognostic formulations of Pan and Ran-
 134 dall (1998) and Wagner and Graf (2010) also consider a constant σ_c , and a steady-state
 135 plume that only interacts with a homogeneous environment. On the other hand, Yano
 136 and Plant (2012a, 2012b) assume that the time evolution of the mass flux is only con-
 137 trolled by the convective cloud cover, but it also considers the steady-state plume model
 138 while completely neglecting any cloud-cloud interaction.

139 Within a diurnal cycle over land, however, if the atmosphere is already unstable
 140 in the morning, the convection develops quite rapidly, while the cloud environment re-
 141 mains rather steady during the day (Tian et al., 2021). In such cases, one can no longer
 142 assume that the convection only interacts with the environment, and thus, convective
 143 memory might be important (Colin et al., 2019; Daleu et al., 2020; Colin & Sherwood,
 144 2021; Hwong et al., 2023). Although the above mentioned prognostic formulations also
 145 introduce convective memory into their formulation, this is achieved based on *ad-hoc*
 146 relations, and not based on physical considerations. The main assumption in these prog-
 147 nostic formulations is that M_c does not respond immediately to changes in the large-
 148 scale state. However, it is not clear why such an assumption might be true for a steady-
 149 state plume that only interacts with a homogeneous environment. In the present work,
 150 we assume that the updraft velocity at cloud base only exhibits a slow change during
 151 the rapid shallow-to-deep transition over land (e.g., Figure 15 of Kurowski et al., 2018),
 152 whereas the cloud fraction of the precipitating clouds evolves from zero in the morning
 153 to a maximum around noon, and thus, for this particular case, the second term in the
 154 rhs of Equation 1 becomes significant. Thus, the scope of this study is to find a dynam-
 155 ical system able to represent the evolution of σ_c during the rapid transition from shal-
 156 low to precipitating convection.

157 To predict the onset of deep precipitating convection, some numerical models as-
 158 sume CIN type triggering functions, which are used to turn on the deep convection scheme
 159 only if the updraft plumes in the boundary layer have a kinetic energy greater than CIN
 160 (Rio et al., 2009, 2013). However, such an implementation does not change the basis of
 161 the parameterization schemes but only decides when the scheme is active or not. If the
 162 scheme assumes a constant σ_c , then σ_c will jump from zero before triggering to a fixed
 163 value at triggering, remaining constant as long as the deep convective scheme is active.
 164 The problem with this kind of triggering function is that it does not allow for deep con-
 165 vection to properly develop from shallow convection, which results in predicting the on-
 166 set of precipitating convection several hours sooner. To ameliorate this problem, several

parameterization schemes assume that within a diurnal cycle, at the triggering, even if CAPE is very large, deep cumulonimbus clouds only form if cold pools are also present (e.g., Hohenegger & Bretherton, 2011; Suselj et al., 2019). However, since CAPE is already large at the triggering time, the convective scheme immediately creates precipitation, being unable to capture the transition from the non-precipitating shallow cumuli to the precipitating congestus clouds. Thus, they are unable to fully correct the time of precipitation onset, but keep the precipitation rate small until the cumulonimbus clouds develop. In this work, we propose a conceptual model for cumulus clouds that allow for a gradual evolution of σ_c when the triggering conditions are met, governed by a predator-prey-type dynamical system.

2 Conceptual Model

In our model the clouds are formed due to the transport of water by the updrafts from the boundary layer. In contrast with the mass-flux formulation, we do not consider that every cloud, or every cloud ensemble, is described by only one steady-state plume, but we consider that a cloud can be formed by the contribution of multiple unsteady convective elements — such as thermals (e.g., Scorer & Ludlam, 1953; Sherwood et al., 2013; Hernandez-Deckers & Sherwood, 2016) or starting plumes (Pinsky et al., 2022) — as also suggested by several authors (e.g., Malkus & Scorer, 1955; Moser & Lasher-Trapp, 2017; Morrison et al., 2020; Vraciu et al., 2023). Indeed, the pulsating behavior of clouds has been documented by both observational studies (e.g., Harrington, 1958; Koenig, 1963; Raymond & Blyth, 1989; Damiani et al., 2006) and numerical simulations (e.g., Zhao & Austin, 2005; Heus et al., 2009; Sakradzija et al., 2015; Peters et al., 2019), which may indicate the presence of successive convective elements within the clouds. Each convective element transports a finite mass of water from the boundary layer to the cloud layer, and the cloud dimension is given by the total amount of water transported by the set of convective elements that reach the condensation level in that given place of the cloud during its life-time, minus the amount of cloud water that evaporates due to mixing with the environment (detrainment). The episodic mixing model of Emanuel (1991) is in fact based on a very similar conceptual picture (see also Emanuel, 1993). Emanuel (1991) makes very clear that in his parameterization scheme, the small convective elements within the clouds are responsible for the convective transport: “I am explicitly attempting to represent the collective effects of an ensemble of individual, $\mathcal{O}(100\text{ m})$ -scale drafts, not of ensembles of $\mathcal{O}(1\text{ km})$ -scale clouds. These drafts, rather than whole clouds, are regarded as the fundamental agents of convective transport.” Thus, in this picture, a cloud can be seen as analogous to a wall of bricks, and a convective element as a new brick fixed on the wall by the builder — the clouds are seen as a collection of water elements brought by a number of convective elements during the cloud life-time, in which every water element represents a brick in our wall. This building process can be visualized for the development of a real cumulonimbus cloud at Kjoenbongarit (2013) or for a congestus cloud at Strong (2017).

We consider here two types of clouds: (i) nonprecipitating shallow cumuli, which are those clouds with a top close to the boundary layer depth, covering a fraction σ_s — this type of clouds remain shallow as they are unable to gain buoyancy, or lose their buoyancy very quickly; and (ii) convective precipitating clouds, which are clouds that are able to gain some buoyancy and have a top much deeper than the boundary layer depth, covering a fraction σ_c . Here, we consider that the convective precipitating clouds have a top above 4 km. Therefore, the total cloud cover is $\sigma = \sigma_s + \sigma_c$. We consider that the difference between the shallow and convective precipitating clouds is that the shallow clouds decay only due to mixing (detrainment) into the environment, whereas the convective precipitating clouds decay also by precipitation. Although the shallow cumuli can also lightly precipitate, we consider that the precipitation rate of shallow cumuli can be neglected with respect to the precipitation rate of convective precipitating clouds.

219 We consider that the total mass m_j of cloud j is given by:

$$m_j = \sum_i^n \delta m_i - m_{D,j}, \quad (2)$$

220 where δm_i is the mass transported into the cloud by the convective element i , n is the
 221 total number of convective elements that contribute to cloud j during its life-time, and
 222 $m_{D,j}$ is the mass lost by the cloud due to mixing with the dry environment and precip-
 223 itation. Here, by cloud mass, we refer to the mass of air within a cloud, but other quan-
 224 tities might be considered as well, such as the mass of condensed particles (water plus
 225 ice), or the total integrated condensed water path. For the whole ensemble of clouds we
 226 can write:

$$m = \sum_j m_j = \bar{\rho} \sigma \overline{\Delta z}, \quad (3)$$

227 where m and $\overline{\Delta z}$ are the total mass and the average depth of the cloud ensemble, respec-
 228 tively, and $\bar{\rho}$ is the mean air density within the clouds. Here, all masses are per unit of
 229 area, so the masses in Equation 2 have units of kg m^{-2} . For the evolution of m , neglect-
 230 ing the time change of $\bar{\rho}$, we thus have:

$$\frac{dm}{dt} = \bar{\rho} \sigma \frac{d\overline{\Delta z}}{dt} + \bar{\rho} \overline{\Delta z} \frac{d\sigma}{dt} = M_0 - D, \quad (4)$$

231 where M_0 is the sum of the contributions from all convective elements to the total mass
 232 flux at the condensation level and $D = d(\sum_j m_{D,j})/dt$, is the rate at which the cloud
 233 ensemble loses mass due to evaporation and precipitation. Therefore, the evolution of
 234 the cloud fraction becomes:

$$\frac{d\sigma}{dt} = \frac{M_0 - D}{\bar{\rho} \overline{\Delta z}} - \sigma \frac{d(\ln \overline{\Delta z})}{dt}. \quad (5)$$

235 For a shallow case at equilibrium, $M_0 - D = 0$, meaning that the new mass brought
 236 into the cloud layer by the convective elements is compensated by the detrainment into
 237 the environment. However, during the shallow-to-deep transition, $\overline{\Delta z}$ increases rapidly,
 238 and the second term in the rhs of Equation 5 is positive and contributes to a reduction
 239 of the total cloud cover. It should be noted that, during the transition, $M_0 - D$ may
 240 not be constant as for a shallow case at equilibrium, but we assume that the contribu-
 241 tion from this term remains generally small compared to the second term in the rhs of
 242 Equation 5. Besides, it is clear that since the first term on the rhs is inversely propor-
 243 tional to $\overline{\Delta z}$, the contribution from $M_0 - D$ to the evolution of σ will decrease as the
 244 cloud layer depth increases. Equation 5 thus indicates that the mass conservation implies
 245 a reduction in the total cloud fraction during the rapid shallow-to-deep transition.

246 2.1 Local Moisture Preconditioning

247 Because the moisture of the cloud environmental layer has been observed to be an im-
 248 portant factor in the transition from shallow to precipitating convection, some studies
 249 argue that the rapid transition from shallow to precipitating convection can be explained
 250 by the moistening of the cloud environment by the shallow cumuli (Holloway & Neelin,
 251 2009; Waite & Khouider, 2010), which is known as the moisture preconditioning mech-
 252 anism. This idea can be perhaps better understood if we consider the following plume
 253 model (Morrison, 2017):

$$\frac{dB}{dz} = -N^2 - \varepsilon B - \varepsilon \frac{gL_v q_{sE}(1 - \mathcal{R}_E)}{c_p T_E \Gamma}, \quad (6)$$

254 where B is the plume buoyancy, z is the vertical coordinate, N^2 is the squared buoyancy
 255 frequency, ε is the entrainment rate, g is the gravitational acceleration, L_v is the latent
 256 heat of vaporization, q_{sE} is the saturation mixing ratio of the environment, \mathcal{R}_E is the
 257 environmental relative humidity, T_E is the temperature of the environment, c_p is the spe-
 258 cific heat of air at constant pressure, and $\Gamma \approx 1 + L_v^2 q_{sE} / (c_p R_v T_E^2)$ is a parameter, for
 259 which R_v is the water vapor gas constant. The last term in the rhs of Equation 6 rep-
 260 represents the cooling rate of the updraft plume due to the evaporation of the cloud water
 261 that mixes with the dry environmental air. Thus, as shallow cumuli continue to increase
 262 RH_E , this term will continue to decrease, allowing the plumes to deepen the cloud layer
 263 (Morrison et al., 2022). However, Hohenegger and Stevens (2013) showed that the mois-
 264 ture preconditioning acts at time scales too long to explain the rapid transition. Note
 265 that the concept of preconditioning as formulated by Waite and Khouider (2010) or Yano
 266 and Plant (2012b) is based on the same consideration as the mass-flux formulation, with
 267 steady plumes that entrains air described by a mean domain value.

268 On the other hand, Vraciu et al. (2023) discussed the role of passive shallow cu-
 269 muli in the transition from shallow to deep convection, which can be regarded as local
 270 moisture preconditioning. As in the moisture preconditioning mechanism described by
 271 (e.g., Waite & Khouider, 2010), the idea is that if the updraft plumes can entrain moister
 272 air, they will be able to grow deeper due to a smaller contribution of the last term in the
 273 rhs of Equation 6. However, the main difference is that we no longer assume a steady-
 274 state plume that entrains air only described by a mean state, as in the mass-flux for-
 275 mulation, but we consider that the plumes (or any other convective elements) have a smaller
 276 life-time than the clouds, and are allowed to develop in the place of existing clouds. Thus,
 277 the cloud itself provides a local preconditioning for the development of the subsequent
 278 convective elements, as also shown by Moser and Lasher-Trapp (2017). This process of
 279 interaction between the convective elements and the existing clouds leads to deeper and
 280 deeper clouds. Furthermore, we can also consider that the clouds, even after a complete
 281 decay, still leave spots of abnormally large humidity that slowly dissipate into the en-
 282 vironment (e.g. Figure 7 of Daleu et al., 2020). Thus, if the convective elements reach
 283 the condensation level in the location of such spots, they will again benefit from the lo-
 284 cal preconditioning, creating deeper clouds. We may also consider that the area of these
 285 spots is proportional to the total cloud cover at the cloud base.

286 Let us consider that at a given time we have a cloud field of shallow cumuli, as schemat-
 287 ically presented in Figure 1A. We consider that every cloud, either shallow or deep, is
 288 formed by a set of convective elements that transported water from the boundary layer
 289 to the cloud layer. After a given time, a new set of convective elements reaches the con-
 290 densation level. Here, we have two possibilities: (i) the convective elements reach the con-
 291 densation level in a place where there are no clouds (or spots of large humidity), form-
 292 ing new shallow cumuli. This case is schematically illustrated in Figure 1B. At the same
 293 time, some of the clouds decay during the development of the new convective elements,
 294 and thus, we can consider that the new clouds statistically replace the old ones that died;
 295 (ii) the new set of convective elements reach the condensation level in the place of an al-
 296 ready existing cloud, as schematically illustrated in Figure 1C. In this case, the convec-
 297 tive elements will transport water from the boundary layer in a higher cloud layer, while
 298 some of the shallow clouds decay. As a result, the total cloud fraction σ decreases, while
 299 the fraction of clouds that become convective σ_c increases.

300 As convection becomes more intense, the compensating entrainment of dry air from
 301 the cloud layer into the boundary layer also increases, which creates a stable transition
 302 layer between the top of the boundary layer z_i and the lifting condensation level (LCL)
 303 (Betts, 1976; Neggers et al., 2006; Albright et al., 2022). As a result, the mass flux of

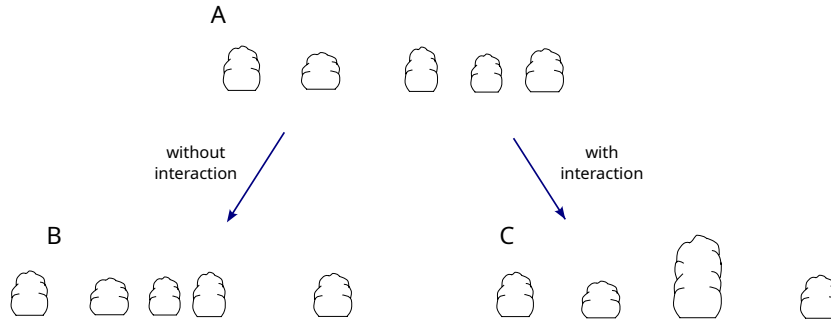


Figure 1. Deepening of a cumulus clouds due to local preconditioning. (A) initial cloud field with five shallow cumuli. (B) after a time, one of the clouds decays, while a new set of convective elements, that do not interact with the existing clouds, forms a new shallow cumulus. As a result, the cloud fraction remains steady. (C) as in (B), but now the new set of convective elements develop in the place of one of the existing clouds, forming a deeper, convective precipitating cloud. As a result, the cloud fraction at cloud base decreases, while the cloud fraction of convective precipitating cumuli increases.

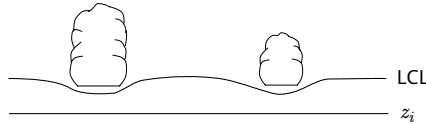


Figure 2. Schematics of non-precipitating clouds altering the transition layer between z_i and LCL.

304 the updrafts at cloud base may also decrease as the number of convective precipitating
 305 clouds increases. Because the non-precipitating clouds always mix with the environment
 306 due to diffusion and turbulent mixing, we expect the air just below the base of a given
 307 non-precipitating cloud to be moister than the air at the same height but in a cloud-
 308 less area (e.g. Albright et al., 2023). Thus, as the convective elements that develop in
 309 the place of an already existing cloud mix moister air than those developing in the cloud-
 310 less areas, we consider that the non-precipitating clouds also create heterogeneity in the
 311 stable transition layer (Figure 2), making easier for the convective elements to reach the
 312 condensation level where there are already non-precipitating clouds present. This altera-
 313 tion of the transition layer is also supported by the findings of Vraciu et al. (2023) who
 314 showed that the fraction of convective elements that develop where a cloud is already
 315 present is comparable with the fraction of convective elements that develop in cloudless
 316 areas, even though the clouds only occupy a very small fractional area. Therefore, we
 317 expect the fraction of updrafts at the cloud base to also decrease with the decrease of
 318 σ , which leads to a further reduction in σ . The local shallow preconditioning thus leads
 319 to deeper clouds, which due to mass conservation and alteration of the transition layer
 320 leads to a reduction in the cloud cover at cloud base.

321 2.2 Cold Pools Feedback

322 Once the clouds begin to precipitate, cold pools are formed in the boundary layer, which
 323 organize the convective field. This organization can be seen as updrafts being larger and
 324 more organized (Schlemmer & Hohenegger, 2014; Meyer & Haerter, 2020). This leads
 325 to further deepening of the cloud layer for two reasons: firstly, the larger convective el-

326 elements experience smaller entrainment (Kurowski et al., 2018; Schlemmer & Hohenegger,
 327 ger, 2014), and thus, are able to better preserve their buoyancy, and secondly, more or-
 328 ganized convective elements facilitate the local preconditioning, as the probability for
 329 a set of convective elements to develop in a certain place (to cluster) is larger. Although
 330 one may argue that the cold pools lead to convective elements that are so large that they
 331 do not require local preconditioning, Savre and Craig (2023) show that, during the tran-
 332 sition, the increase in the updraft dimension is negligible compared with the increase in
 333 cloud dimension — there are no updrafts as large as a deep convective cloud, and thus,
 334 we argue here that cold pools essentially make the local preconditioning more efficient
 335 without substantially altering the properties of the boundary layer updrafts. In other
 336 words, we still consider that a convective cloud is a result of multiple convective elements
 337 bringing water from the boundary layer in the same location, but since the convective
 338 elements are larger and better organized, a smaller number of convective elements are
 339 required to build a precipitating cloud. Following the analogy between clouds and brick
 340 walls, we can picture the cold pool feedback as having sets of bricks that are already tied
 341 together, and thus, the building process is much more efficient since the builder brings
 342 a new set of tied bricks with only one move. Although we do not consider that it is im-
 343 possible for only one convective element to create a precipitating cloud, we consider that
 344 even in this case, the convective element will benefit from the large humidity spots cre-
 345 ated by the non-precipitating clouds, and such a situation might rather correspond to
 346 the creation of “turkey towers” (e.g. Figure 7.14 in Markowski & Richardson, 2011), rather
 347 than the creation of congestus or cumulonimbus clouds.

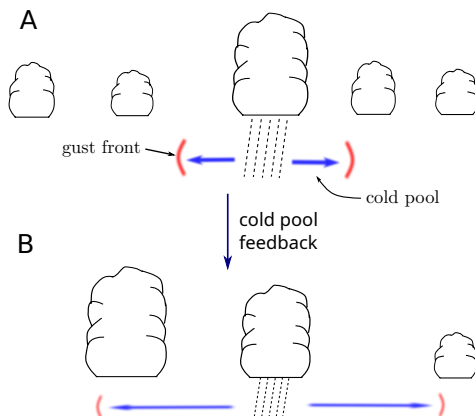


Figure 3. Deepening of a cumulus clouds due to cold pool feedback. (A) initial cloud field with four shallow clouds and one convective cloud in the decaying precipitating stage, which creates a cold pool that leads to the development of a new convective precipitating cloud at a later time (B). At the same time, some of the shallow clouds decay without being replaced by new shallow cumuli. As the precipitating clouds, being deeper, occupy a smaller fraction than the shallow cumuli, for the same amount of building convective elements, the total cloud cover decreases.

348 In Figure 3, we illustrate the effect of the cold pools in the deepening of subsequent
 349 convection. Initially, we consider a field of shallow and precipitating clouds. The pre-
 350 cipitating cloud illustrated in Figure 3A precipitates, creating a cold pool, and a new con-
 351 vective precipitating cloud is formed later on, as schematically illustrated in Figure 3B.
 352 Since the convective elements are larger and more organized, more water is transported
 353 by them to higher altitudes, which leads to a net decrease in the total cloud field. More-
 354 over, although the cold pools trigger new updrafts at their gust fronts (Torri et al., 2015;
 355 Meyer & Haerter, 2020), as the cold pools represent areas of evaporatively cooled down-

356 drafts they also inhibit updrafts from developing within these areas. The cold pools thus
 357 make the convective elements to be fewer but stronger (e.g. Figure 15 of Kurowski et
 358 al., 2018). Therefore, we also expect a reduction in the updraft fraction at the cloud base
 359 due to cold pool feedback.

360 2.3 Predator-Prey Model

361 The physical processes discussed above suggest that the transition from shallow to pre-
 362 cipitating convection can be modeled as a predator-prey process with convective precip-
 363 itating clouds acting as predators, and the total cloud field acting as prey. We consider
 364 that the prey is represented by the total cloud field as both the shallow and convective
 365 precipitating clouds precondition their local environment, as long as the convective pre-
 366 cipitating clouds are not in the decaying precipitating stage. However, we consider that
 367 the fraction of clouds in the decaying precipitating stage is much smaller than the total
 368 cloud fraction.

369 Here, for simplicity, we consider a very simple predator-prey model, namely the
 370 Lotka-Volterra model (Takeuchi, 1996), given by:

$$\frac{dx}{dt} = ax - bxy, \quad (7)$$

$$\frac{dy}{dt} = exy - fy, \quad (8)$$

371 where x is the population of prey and y is the population of predators, and a , b , e , and
 372 f are system coefficients. A solution of the Lotka-Volterra system is presented in Fig-
 373 ure 4.

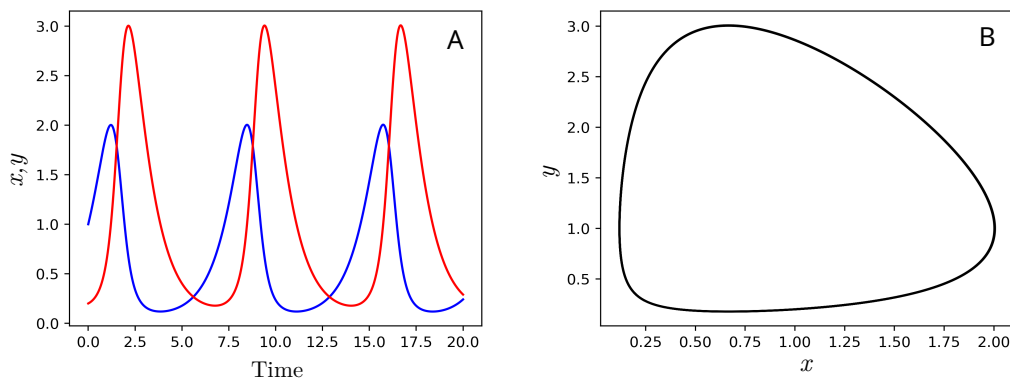


Figure 4. Solution of the Lotka-Volterra system. (A) Time evolution of prey (blue solid line) and predators (red solid line); (B) Limit cycle of the system.

374 In our case, we consider that the prey is played by the total cloud population at
 375 cloud base, which sustains the development of the deeper clouds, that act as predators.
 376 Thus, we consider $x = \sigma$ and $y = \sigma_c$. The first term in the rhs of Equation 7 repre-
 377 sents the difference between the source of new convective elements from the boundary
 378 layer and the decay of the old clouds due to the mixing with the environment and pre-
 379 cipitation. In the absence of precipitation, all the clouds are shallow. As shallow cumuli
 380 moisten their environment, we expect the shallow cloud cover to increase as the life-time

381 of the clouds increases due to mixing with moister and moister air. Thus, in the absence
 382 of precipitation, the shallow cloud cover grows exponentially, which might correspond
 383 to a cumulus-to-stratiform transition, rather than the case considered here. The sec-
 384 ond term represents the decay in the cloud cover due to interactions between precipi-
 385 tating clouds and the rest of the cloud population. σ_c appears in this term for two rea-
 386 sons: firstly, the deeper clouds have longer life-times and are wider, hence increasing the
 387 probability for new convective elements to interact with them, and secondly, when they
 388 precipitate, they form cold pools that trigger new precipitating clouds thus further de-
 389 creasing the total cloud cover (see Section 2.2). The first term on the rhs of Equation
 390 8 represents the growth of convective precipitating clouds for the same physical argu-
 391 ments as for the second rhs term of the prey equation. Lastly, the last term in the rhs
 392 of Equation 8 represents the decay rate of convective precipitating clouds due to precip-
 393 itation and dissipation into the environment. An important limitation of the Lotka-Volterra
 394 model, however, is that predators cannot be created from nothing, and thus, σ_c must be
 395 initialized with a nonzero value. Note that the predator-prey system described here com-
 396 prises cannibalism as the total cloud population, including precipitating clouds, acts as
 397 a prey for the precipitating cloud population.

398 Although more realistic and accurate predator-prey models may be considered here,
 399 the Lotka-Volterra model was selected for its simplicity. Besides, it should be kept in
 400 mind that the coefficients of the predator-prey system may not be universal, but may
 401 rather depend on other meteorological parameters, such as environmental relative hu-
 402 midity, or the boundary layer depth, which are well-known to be important parameters
 403 in the shallow-to-deep transition (e.g., Morrison et al., 2022; Grabowski, 2023).

404 Similar predator-prey models for the cloud-precipitation system have previously
 405 been formulated by Colin and Sherwood (2021) and Koren and Feingold (2011), but based
 406 on completely different physical arguments, and not for the specific transition case dis-
 407 cussed here. Our model also differs from the predator-prey model of Wagner and Graf
 408 (2010) where a Lotka-Volterra model was used to model interactions between cloud species,
 409 excluding cannibalism.

410 **3 Tests and Extensions of the Predator-Prey Model**

411 **3.1 LBA Transition Case**

412 Results obtained from a high-resolution large-eddy simulation (LES) were analysed in
 413 order to test our hypotheses. The model configuration constitutes an idealization of the
 414 original Large-scale Biosphere-Atmosphere (LBA) case described in Grabowski et al.
 415 (2006) with initial conditions and forcings taken from Böing et al. (2012). The relative
 416 humidity was held constant and equal to 80% up to an altitude of 6,000 m, and then
 417 decreased linearly to 15% at 17,500 m. The potential temperature was computed from
 418 a prescribed lapse rate following a simple function of altitude, while horizontal winds were
 419 initially set to 0 m s⁻¹ everywhere. Latent and sensible surface heat fluxes were held con-
 420 stant throughout the simulation and equal to 343 W m⁻² and 161 W m⁻² respectively,
 421 which corresponds to the diurnal averages of the time-dependent fluxes imposed in Grabowski
 422 et al. (2006). Horizontal winds were nudged back to their initial values with a time scale
 423 of 6 hr over the course of the simulation, but no other external forcing (including radi-
 424 ation and large-scale advection) was imposed.

425 The simulation was performed using the MISU-MIT Cloud and Aerosol model (MIMICA;
 426 Savre et al., 2014) as described in Savre and Craig (2023). The numerical domain ex-
 427 tends over 102.4 km in both horizontal directions, and the upper boundary is situated
 428 14,250 m above the surface. The horizontal grid spacing is equal to 100 m in both di-
 429 rections, while the vertical grid spacing is constant and equal to 25 m below 1500 m, but
 430 increases geometrically above to reach ~ 400 m in the topmost grid layer. Lateral bound-

431 aries are periodic, whereas the surface is considered as a free-slip boundary (no momen-
 432 tum fluxes).

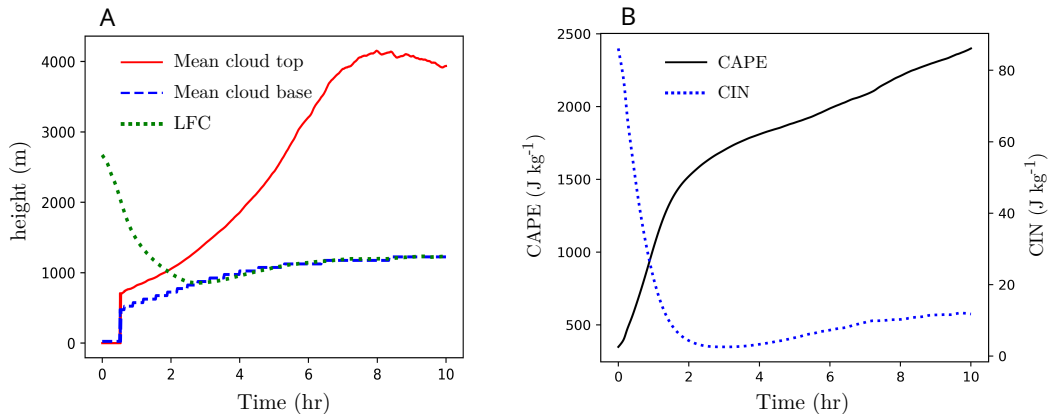


Figure 5. Shallow-to-deep transition in the idealized LBA case. (A) Time series of mean cloud top (red solid line), mean cloud base (blue dashed line), and LFC (green dotted line). (B) Time series of CAPE (black solid line) and CIN (blue dotted line).

433 The simulation was continued over a period of 10 hr, during which time-dependent
 434 variables were extracted every minute. The first clouds are observed 1 hr after the start
 435 of the simulation, whereas the onset of surface precipitation occurs 1.5 hr later. Over-
 436 all, the transition from shallow-to-deep convection happens progressively over the first
 437 7 hr of simulation. In Figure 5A, the mean cloud base and mean cloud top altitudes are
 438 shown. Here, the mean cloud base is defined as the level at which the cloud cover is max-
 439 imum, and the mean cloud top is defined as the first vertical layer from the top where
 440 the condensed water mixing ratio exceeds $10^{-3} \text{ g kg}^{-1}$. Clouds are identified at locations
 441 where the condensed water mixing ratio exceeds a threshold of $10^{-3} \text{ g kg}^{-1}$. In addition,
 442 the level of free convection (LFC) is also represented. As one may see, after around 3
 443 hr the mean cloud base altitude is almost identical to the LFC. The time evolution of
 444 CAPE and CIN is also represented in Figure 5B. CIN becomes very small after 2 hr, grad-
 445 ually increasing during the shallow-to-deep transition to about 10 J kg^{-1} . Here, we con-
 446 sider the shallow-to-deep convection transition to begin 2.5 hr after the start of the sim-
 447 ulation. During the transition, CAPE increases from about 1600 J kg^{-1} to about 2000
 448 J kg^{-1} .

449 The total cloud cover σ and cloud cover associated with precipitating convection
 450 σ_c that will be used to validate the predator-prey model are defined as follows. The to-
 451 tal cloud cover is computed as the ratio between the number of grid cells identified as
 452 cloudy at the mean cloud base altitude to the total number of grid cells at that level.
 453 The cloud cover of convective precipitating clouds is defined following the same proce-
 454 dure but 4 km above the surface. In Figure 6A, simulated total and precipitating cloud
 455 covers are shown together with a solution of the Lotka-Volterra model in which the cloud
 456 fraction at cloud base (total cloud population) is assumed to act as prey, and the cloud
 457 fraction at 4 km (precipitating cloud population) is assumed to act as predator. The Lotka-
 458 Volterra model is solved using the simple Euler method with 10^4 iterations (a conver-
 459 gence test with 10^3 iterations has been performed, showing no significant difference). Here,
 460 the Lotka-Volterra model is represented only to show the predator-prey characteristic
 461 of the system, and thus, no objective tuning of coefficients against the LES data has been
 462 performed: the coefficients were simply chosen to visually match the LES data. As can
 463 be seen from Figure 6A, even a very simple predator-prey system can model reasonably

464 well the rapid transition from shallow to deep continental convection, however, far from
 465 being a perfect model. As speculated above, σ_c can indeed act as a predator. We show
 466 in particular that the cloud cover decreases as the fraction of convective clouds at a higher
 467 level increases. Later, as the total cloud cover decreases, the number of clouds that pro-
 468 vide local preconditioning for the subsequent convection also decreases, and thus, the pop-
 469 ulation of predators (precipitating clouds) will decrease as they no longer have enough
 470 preys to feed on.

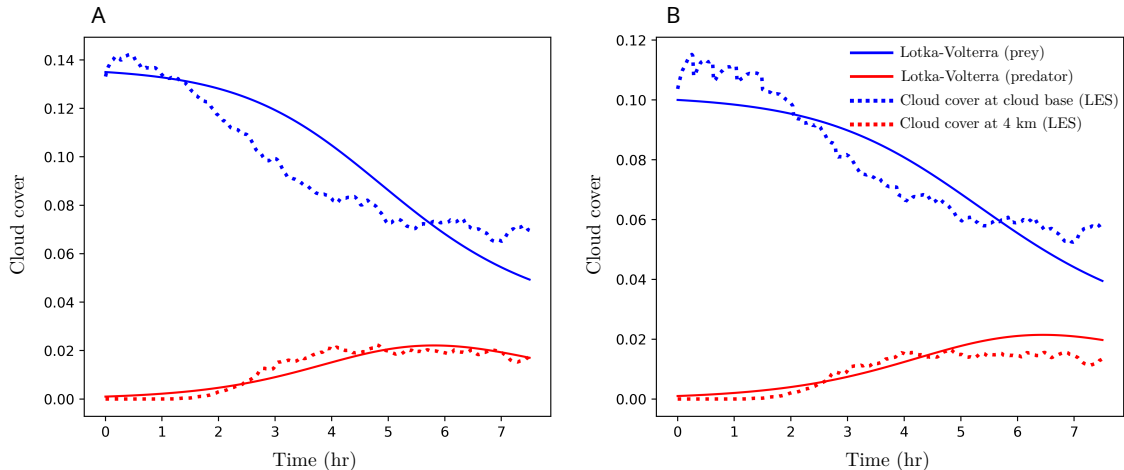


Figure 6. Lotka–Volterra model (solid lines) vs. LES data (dotted lines) for the LBA transi-
 tion case. (A) Cloud cover at the cloud base as prey (blue lines) and cloud cover at 4 km height
 as predators (red lines). (B) As in (A) but for cloudy updraft cover. For the Lotka–Volterra
 model, the following coefficients are considered: $a = 0$, $b = 3 \cdot 10^{-3} \text{ s}^{-1}$, $e = 3.5 \cdot 10^{-3} \text{ s}^{-1}$,
 $f = 2.5 \cdot 10^{-4} \text{ s}^{-1}$ (A); and $a = 0$, $b = 3 \cdot 10^{-3} \text{ s}^{-1}$, $e = 4 \cdot 10^{-3} \text{ s}^{-1}$, $f = 2 \cdot 10^{-4} \text{ s}^{-1}$ (B). The
 initial conditions are set to 0.135 for the cloud cover at the cloud base, 0.1 for the cloudy updraft
 cover at the cloud base, and 10^{-3} for the cloud cover and for the cloudy updraft at 4 km. Here,
 the initial time is set to 2.5 hr after the start of the simulation.

471 Because the cloudy updrafts are regarded as the fundamental agents of vertical con-
 472 vective transport in the mass–flux parameterization, we also analyze here the predator–
 473 prey characteristics of cloud cover with clouds identified based on an additional updraft
 474 criterion. Here, a threshold of 0.1 m s^{-1} is used to identify the cloudy updrafts. The predator–
 475 prey characteristics of cloud cover based on this additional updraft criterion (cloudy up-
 476 draft cover) are presented in Figure 6B. As speculated above, the cloudy updrafts cover
 477 also follows predator–prey characteristics, like the total cloud population. The predator–
 478 prey characteristics can be seen from the fact that the cloudy updraft cover at cloud base
 479 decreases as the cloudy updraft cover at 4 km increases in the first part of the transi-
 480 tion. This is followed by a decrease in the cloudy updraft cover at 4 km as the number
 481 of prey becomes too small. Note that Yano and Plant (2012b) argue that during the shallow–
 482 to–deep transition, as CAPE increases, the cloudy updraft cover at cloud base also in-
 483 creases, but without giving any physical argument to support this assertion. However,
 484 it is quite clear from Figure 6B that for the rapid shallow–to–deep transition discussed
 485 here, the cloud cover at the cloud base exhibits a decrease during the transition, even
 486 though CAPE does increase.

487 As a first order approximation, we can consider that the surface precipitation rate
 488 P is directly proportional to σ_c . Similar to Koren and Feingold (2011), we may there-

489 fore replace σ_c with P in equations 7–8, thus considering that the surface precipitation rate acts as a predator that preys on the total cloud fraction. We then expect to see a
 490 time series for the cloud–precipitation system resembling that displayed on Figure 4A,
 491 and a solution for the cloud cover and precipitation rate similar to the one showed on
 492 Figure 4B.
 493

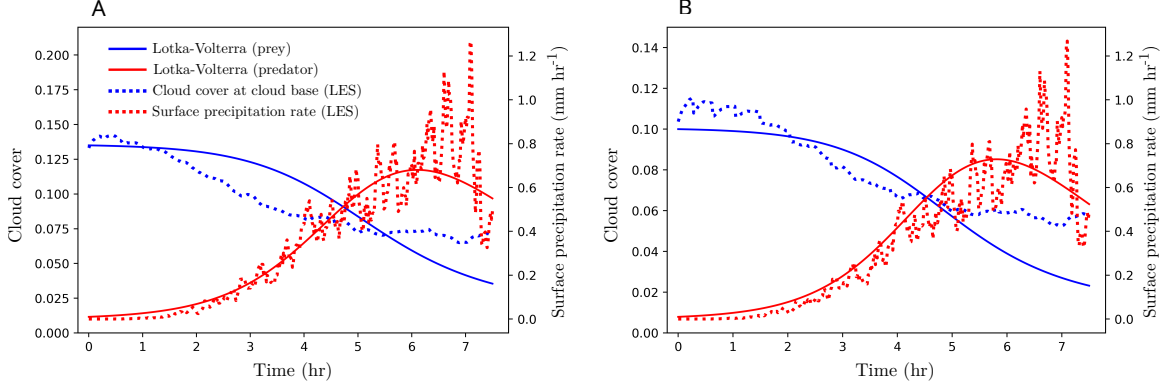


Figure 7. As in Figure 6 but the with surface precipitation rate acting as predators. For the Lotka–Volterra model, the following coefficients are considered: $a = 0$, $b = 1.5 \cdot 10^{-4} \text{ hr mm}^{-1} \text{ s}^{-1}$, $e = 3.5 \cdot 10^{-3} \text{ s}^{-1}$, $f = 2 \cdot 10^{-4} \text{ s}^{-1}$ (A); and $a = 0$, $b = 1.5 \cdot 10^{-4} \text{ hr mm}^{-1} \text{ s}^{-1}$, $e = 5 \cdot 10^{-3} \text{ s}^{-1}$, $f = 2.1 \cdot 10^{-4} \text{ s}^{-1}$ (B). The initial surface precipitation rate is set to $10^{-3} \text{ mm hr}^{-1}$.

494 In Figure 7, the time series of cloud cover at cloud base and surface precipitation
 495 rate are presented, together with a solution of the Lotka–Volterra model in which the
 496 cloud fraction at cloud base is assumed to act as prey, and the surface precipitation rate
 497 is assumed to act as predator. The surface precipitation rate displayed in Figure 7 rep-
 498 represents the domain–averaged surface precipitation rate. Indeed, the cloud–precipitations
 499 system exhibits predator–prey characteristics during the rapid shallow–to–deep transi-
 500 tion, as speculated above. Although not perfect, the Lotka–Volterra model does seem
 501 to represent reasonably well the interaction between clouds and precipitation.

502 3.2 Extension to a three species model

503 An extension to a three species model can be made by considering that the convective
 504 precipitating clouds can be further classified as congestus and cumulonimbus clouds. Here,
 505 we consider that the congestus clouds are those clouds with a top between 4 km and 8
 506 km, whereas the cumulonimbus clouds have a top above 8 km. Therefore, we consider
 507 that the cloud cover at the cloud base (total cloud population) acts as prey for the cloud
 508 cover at 4 km σ_c (convective precipitating cloud population), which also represents the
 509 prey for the cloud cover at 8 km σ_{cb} (cumulonimbus cloud cover). Hence, we have the
 510 following predator–prey system:

$$\frac{d\sigma}{dt} = \beta_1\sigma - \beta_2\sigma\sigma_c, \quad (9)$$

$$\frac{d\sigma_c}{dt} = \beta_3\sigma\sigma_c - \beta_4\sigma_c\sigma_{cb} - \beta_5\sigma_c, \quad (10)$$

$$\frac{d\sigma_{cb}}{dt} = \beta_6\sigma_c\sigma_{cb} - \beta_7\sigma_{cb}, \quad (11)$$

511 where β_1 – β_7 are system coefficients. A solution to this system is presented in Figure 8,
 512 together with time series of cloud cover at the cloud base (Figure 8A), 4 km (Figure 8B),
 513 and 8 km (Figure 8C), from the LBA transition case described above. Comparing the
 514 LES data for the cloud cover at these three levels with the solution of the Lotka–Volterra
 515 model, the system seems to exhibit predator–prey characteristics with three species.

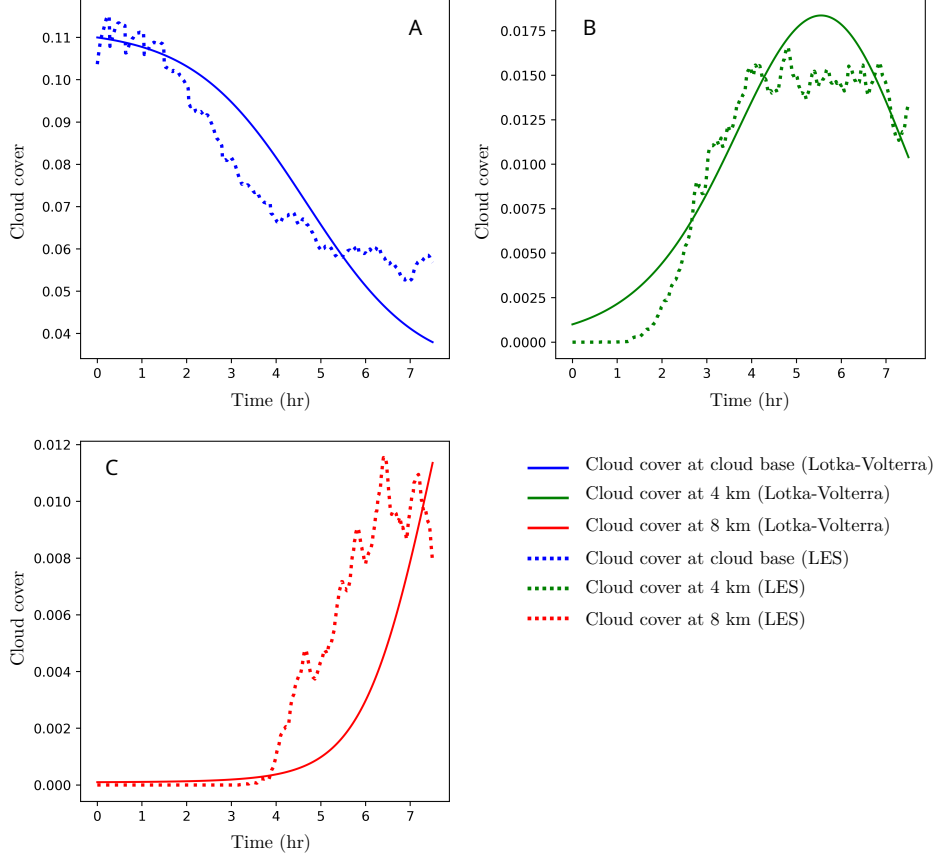


Figure 8. Three species Lotka–Volterra model (solid lines) vs. LES data (dotted lines) for the LBA transition case. (A) Cloudy updraft cover at the cloud base as prey (blue lines); (B) Cloudy cover at the 4 km height representing the convective fractional area of congestus and cumulonimbus clouds; (C) Cloudy cover at the 8 km height representing the convective fractional area of cumulonimbus clouds. For the Lotka–Volterra model, the following coefficients are considered: $\beta_1 = 0$, $\beta_2 = 3.8 \cdot 10^{-3} \text{ s}^{-1}$, $\beta_3 = 3.8 \cdot 10^{-3} \text{ s}^{-1}$, $\beta_4 = 10^{-2} \text{ s}^{-1}$, $\beta_5 = 2 \cdot 10^{-4} \text{ s}^{-1}$, $\beta_6 = 1.7 \cdot 10^{-2} \text{ s}^{-1}$, $\beta_7 = 10^{-6} \text{ s}^{-1}$. The initial conditions are set to 0.11, 10^{-3} , and 10^{-4} for the cloudy updraft cover at the cloud base, at 4 km, and 8 km, respectively.

516 Further extension to n_z species, where n_z represents the number of vertical levels
 517 used by the parent numerical model, follows immediately. For the updraft fractional area
 518 σ_k at the vertical level k , we now have:

$$\frac{d\sigma_k}{dt} = a_{k,k-1}\sigma_k\sigma_{k-1} - a_{k,k+1}\sigma_k\sigma_{k+1} + r_k\sigma_k, \quad (12)$$

519 where $a_{k,k-1}$, $a_{k,k+1}$, and r_k are system coefficients. The number of species represents
 520 the number of vertical levels of the parent numerical model between LFC and the equi-
 521 librium level.

522 3.3 LBA Transition Case with Suppressed Cold Pools

523 As discussed in Section 2, in our conceptual model, the predator–prey characteristics for
 524 the shallow–to–deep transition is due to the local moisture preconditioning, with the cold
 525 pool feedback only acting as a reinforcement. Thus, we argue that predator–prey behav-
 526 ior is expected even in the absence of the cold pools. To test this aspect, an additional
 527 simulation with suppressed cold pools is performed. The strategy proposed by Böing et
 528 al. (2012) was adopted here whereby potential temperature and water vapor mixing ra-
 529 tio tendencies below cloud base are nudged to their horizontally averaged values with
 530 a time scale of 10 min.

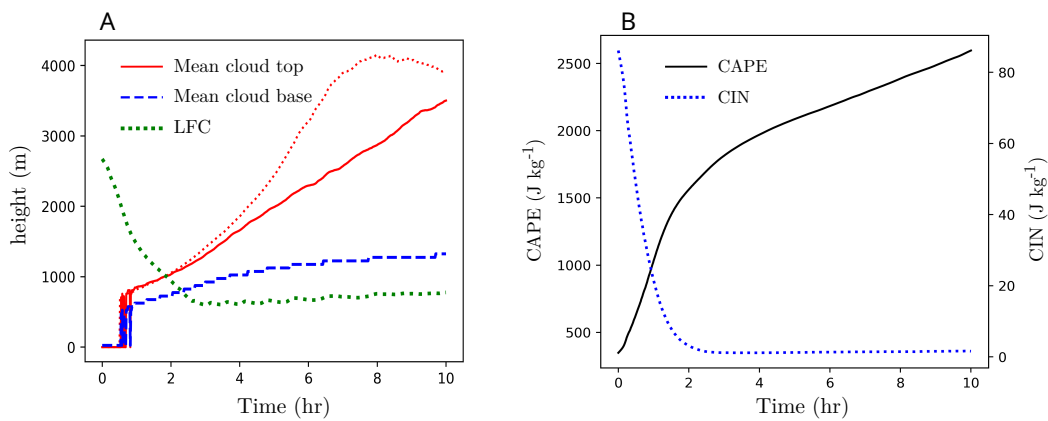


Figure 9. As in Figure 5, but for the case with suppressed cold pools. The mean cloud top for the case with active cold pools is also displayed here with red dotted line.

531 In Figure 9A, the mean cloud top, mean cloud base, and LFC are presented. The
 532 mean cloud top for the case with active cold pools is also presented here to better ap-
 533 preciate the cold pool feedback in the shallow–to–deep transition. As expected, the tran-
 534 sition is slower for the case with suppressed cold pools, although there is not a large dif-
 535 ference between the mean cloud top for the two cases in the first part of the transition,
 536 during which we argue that the role of local preconditioning is the main mechanism re-
 537 sponsible for the transition. As another interesting aspect, in this case, the LFC is lower
 538 than the mean cloud base during the shallow–to–deep transition. As in the case with ac-
 539 tive cold pools, we consider that the transition starts at 2.5 hr after the start of the simu-
 540 lation, but the cloud top does not reach a maximum even after 10 hr, at the end of the
 541 simulation. The time series for CAPE and CIN is represented in Figure 9B. Although
 542 CAPE increases in a similar fashion to the case with active cold pools, CIN reaches a
 543 minimum after around 2.5 hr, remaining rather constant during the transition, at a value
 544 of about 1.5 J kg^{-1} . In addition, LFC is also much lower in the case with suppressed cold
 545 pools (around 0.7 km) than in the case with active cold pools (around 1 km).

546 In Figure 10, the cloudy updrafts covers at cloud base, 4 km, and 8 km, are repre-
 547 sented for the case with suppressed cold pools, together with a solution of the three species
 548 Lotka–Volterra model. As speculated, even without cold pools, the system seems to ex-
 549 hibit predator–prey characteristics. In order to appreciate the role of the cold pool feed-
 550 back in the transition, we also represent the cloudy updrafts covers for the case with ac-

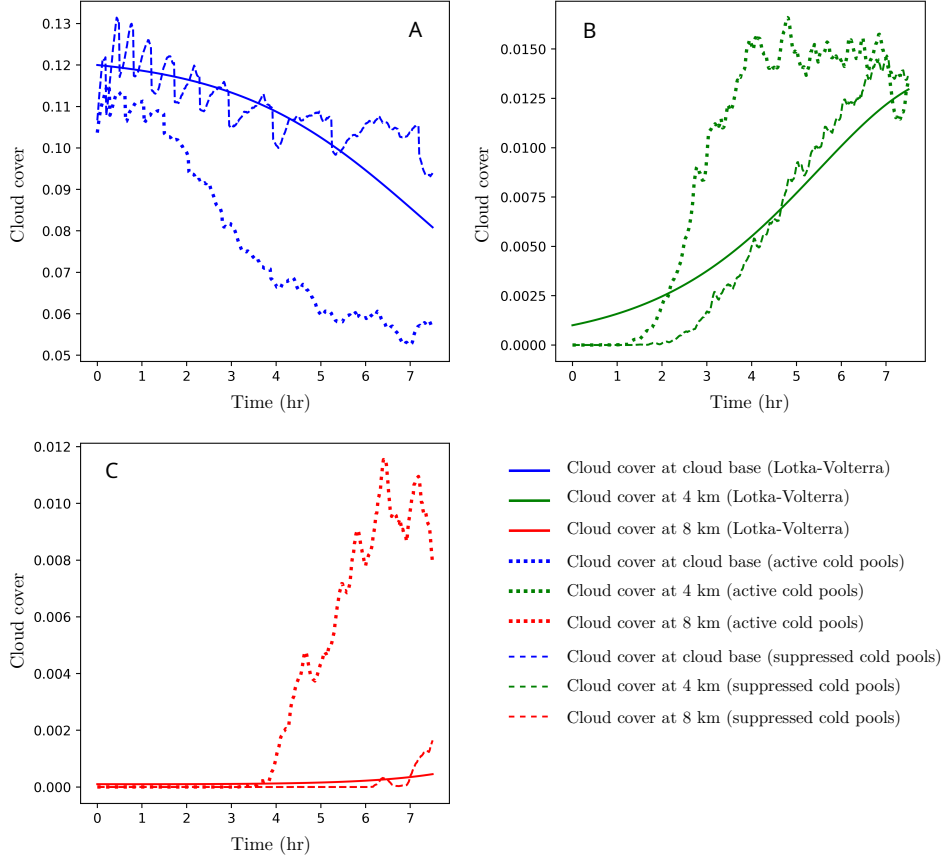


Figure 10. As in Figure 8, but for the case with suppressed cold pools. The cloudy updraft covers for the case with active cold pools are also displayed here with dotted lines, while the cloudy updraft covers for the case with suppressed cold pools are represented with dashed lines. For the Lotka–Volterra model, the following coefficients are considered: $\beta_1 = 0$, $\beta_2 = 2.5 \cdot 10^{-3} \text{ s}^{-1}$, $\beta_3 = 2.5 \cdot 10^{-3} \text{ s}^{-1}$, $\beta_4 = 10^{-2} \text{ s}^{-1}$, $\beta_5 = 1.7 \cdot 10^{-4} \text{ s}^{-1}$, $\beta_6 = 1.3 \cdot 10^{-2} \text{ s}^{-1}$, $\beta_7 = 2 \cdot 10^{-5} \text{ s}^{-1}$. The initial conditions are set to 0.12, 10^{-3} , and 10^{-4} for the cloudy updraft cover at the cloud base, at 4 km, and 8 km, respectively.

551 tive cold pools. As we expected from the conceptual model, without cold pool feedback
 552 the predators are not that efficient in preying on the total cloud population, and thus
 553 the cloud cover at the cloud base does not decrease as fast as the cloud cover for the case
 554 with active cold pools, while the populations of convective precipitating clouds and cumulonimbus clouds are not able to grow as fast and as much as for the case with active
 555 cold pools. Moreover, with suppressed cold pools, a larger number of updrafts are able
 556 to reach the condensation level as CIN is lower and there is no organization of the updraft
 557 field in the boundary layer.
 558

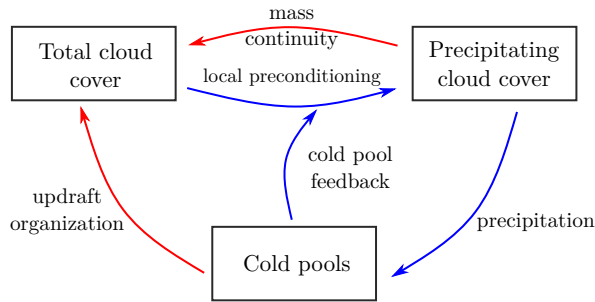


Figure 11. Schematics of feedback between the clouds and cold pools. The blue arrow denotes a positive causality, while the red one denotes a negative causality.

559 Although there is a significant difference in the number of cumulonimbus clouds
 560 between the two simulations, it is clear that the deepening of cumulus convection is possible even without cold pools feedback. This aspect, together with the predator–prey characteristics of the case with suppressed cold pools, indicates that the local preconditioning plays a major role in the shallow–to–deep transition, as also argued by Vraciu et al. (2023), and we believe that much more attention should be given to the local moisture preconditioning, and to the interplay between the local preconditioning and cold pools feedback during the transition from shallow to precipitating convection. We schematically present the feedback loops between the clouds and cold pools in our conceptual model on Figure 11. A negative feedback loop between the total cloud cover and precipitating cloud cover is possible without the presence of the cold pools, due to local preconditioning and mass continuity, implying a predator–prey–type of interaction between the two. As the precipitating clouds start to precipitate in their decaying state, cold pools are formed in the boundary layer, which have a positive effect on the population of precipitating clouds, but also a direct negative effect on the total cloud cover due to the organization of updrafts in the boundary layer, as discussed in Section 2.2. As the cold pools have a positive feedback on the population of precipitating clouds, due to mass continuity, the cold pools also have an indirect negative effect on the total cloud cover, as also schematically illustrated in Figure 3. Here, the arrow of the cold pools feedback points towards local preconditioning, as in our conceptual model the cold pools, through the organization of updrafts, increase the probability of updrafts feeding into preexisting clouds, and thus, leading to a larger degree of local preconditioning, as also discussed in Section 2.2. Overall, the cold pools amplify the feedback loop between the total cloud cover (prey) and the precipitating cloud cover (predator), which can be seen as making the predators more efficient in catching the prey. In this sense perhaps, the cold pools may be seen as mountains forcing the preys and predators to live into narrow valleys (the gust fronts), thus facilitating the interactions between them.
 585

586

3.4 Complete Diurnal Cycle

587

588

589

590

591

592

593

594

595

To see if within a complete diurnal cycle the cloud–precipitation system exhibits predator–prey characteristics, we consider here the idealized case reported in Jensen et al. (2022) that is openly available at Haerter (2021). The reader is referred to Jensen et al. (2022) for case description and methodological details. In a complete diurnal cycle, we can no longer ignore the contribution of the surface heat flux on σ . Thus, we can no longer assume that the Lotka–Volterra system, in which there is no external forcing, can describe the interaction between the cloud cover and precipitation rate. However, during the transition from shallow to precipitation convection, we still expect to see a predator–prey type of interaction.

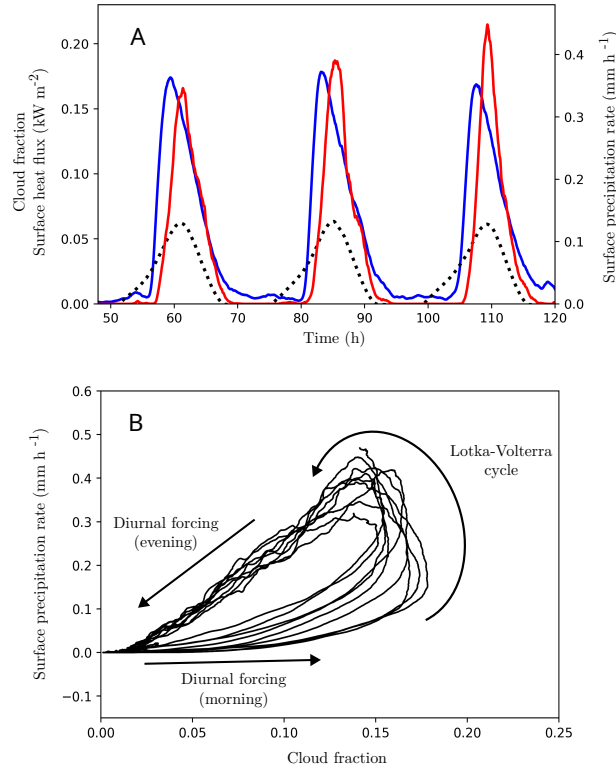


Figure 12. Large-eddy simulation of the cloud–precipitation system in a complete diurnal cycle from Jensen et al. (2022). (A) Time series for cloud fraction (blue solid line) and surface precipitation rate (red solid line) for three complete diurnal cycles. The surface heat flux is also represented for reference (dotted black line). (B) Limit–cycle of the cloud–precipitation system for the complete simulation (10 days), except the first two days, which are considered spin–up time.

596

597

598

599

600

601

602

603

In Figure 12, the LES data for cloud cover and surface precipitation from Jensen et al. (2022) are represented. In the morning, during the onset of the shallow convection, the cloud population increases as more and more updrafts are able to overcome the transition layer and reach the condensation level, and thus, the evolution of the cloud fraction is dominated by the diurnal forcing associated with the surface fluxes. As CIN approaches zero, the transition from shallow to precipitation convection starts, and indeed, during this short period, we see predator–prey characteristics in the cloud–precipitation system (Figure 12A), which correspond to the upper–right portion of the limit–cycle (Fig-

604 ure 12B). Thus, during the transition, in agreement with our conceptual model, the cloud
 605 fraction decreases as the precipitation rate increases, which in turn leads to a reduction
 606 in the precipitation rate. During the evening, as the surface heat flux is unable to pro-
 607 vide enough energy into the system, and CIN is slowly restored. Thus, the cloud frac-
 608 tion decreases as the clouds that decay are no longer replaced by new active clouds, and
 609 the cloud population is again controlled by the diurnal forcing.

610 Although Figure 12 suggests that even within a complete diurnal cycle the system
 611 exhibits predator–prey characteristics, our simple Lotka–Volterra model is only able to
 612 represent the transition phase happening during the day. The model is indeed unable
 613 to represent the simultaneous decay of both shallow and deep cumuli at night when the
 614 reduced surface fluxes cannot sustain convection. A predator–prey model that takes into
 615 consideration this diurnal forcing might however be designed and adjusted to reproduce
 616 the complete diurnal cycle of cloud and precipitation. In this context, surface fluxes might
 617 be modeled as an external food supply for the preys in a biological system.

618 4 Discussion and Conclusions

619 In this study, we consider that the cumulus clouds are formed due to the upward trans-
 620 port of water vapor from the boundary layer by multiple convective elements, as sug-
 621 gested by empirical evidence. As the clouds themselves precondition their local surround-
 622 ings for the subsequent convective updrafts, it is considered that the convective precip-
 623 itating clouds act as predators, eating from the total cloud fraction that sustains their
 624 growth. As the clouds become deeper, the total cloud fraction decreases, and thus, the
 625 total cloud population can be seen as the prey population in a predator–prey system.
 626 It is also argued that the cold pool feedback acts as a reinforcement mechanism, lead-
 627 ing to more clustered convection. The conceptual picture for the shallow-to-deep con-
 628 vection reminds us of the transition from unorganized to aggregated convection, but at
 629 a smaller scale. Therefore, we argue that the very complex cloud dynamics in the rapid
 630 shallow-to-deep transition of atmospheric convection can be described by the very sim-
 631 ple Lotka–Volterra predator–prey system if it is assumed that the change in the large-
 632 scale state is slow enough during the transition. We tested a simple predator–prey model
 633 against idealized high-resolution LES data, showing good agreement between them. To
 634 isolate the role of local moisture preconditioning from that of cold pool feedback, we also
 635 consider a twin LES simulation with suppressed cold pools. In agreement with our con-
 636 ceptual model, the transition displays predator–prey characteristics even without cold
 637 pools, which might be an indication that the local preconditioning plays an important
 638 role in the shallow-to-deep transition. Finally, we discuss the complete diurnal cycle of
 639 deep convection, showing that the cloud population also exhibits a predator–prey-type
 640 of behavior in this situation. We consider that future research is required to study in depth
 641 every causality implied by our study, which might help us better understand the com-
 642 plex process of storm formation and convective organization.

643 In a diurnal cycle of deep continental convection, the predator–prey model assumes
 644 a gradual transition to deep convection instead of assuming an instantaneous deep con-
 645 vection triggering. The majority of current mass–flux schemes for deep convection con-
 646 sider a constant fractional area occupied by the convection, either explicitly or implic-
 647 itly. However, in a rapid transition from shallow to precipitating deep convection, the
 648 environmental state only exhibits a small change, and the convective mass–flux is pri-
 649 marily controlled by convective fractional area and not by the vertical velocity. There-
 650 fore, our predator–prey model may be implemented for such a case by replacing the mass-
 651 flux predicted by the deep convection scheme M'_c with an adjusted mass–flux $M_{c,adj}$, as
 652 follows:

$$M_{c,adj} = \frac{\sigma_c}{\sigma'_c} M'_c, \quad (13)$$

653 where σ_c is the fraction of convective precipitating clouds from the predator–prey model,
 654 and σ'_c is the constant fractional area assumed by the deep convection schemes. If the
 655 scheme does not assume a fractional area in an explicit way, then a constant value for
 656 σ'_c must be prescribed. Therefore, a predator–prey model may be implemented in a weather
 657 prediction or climate numerical model, obtaining a cumulus parameterization scheme with
 658 convective memory, that is based on a more realistic conceptual picture than the tradi-
 659 tional mass–flux formulation, that goes beyond the one-cloud equals one-updraft frame-
 660 work. It should be noted, however, that this implementation cannot be made if the deep
 661 convective scheme already has a parameterization for the cold pool feedback (e.g., Rio
 662 et al., 2009; Suselj et al., 2019), as this would lead to a ‘double counting’ of the cold pools
 663 effect. Such an implementation, however, can only be made during the shallow–to–deep
 664 transition, as it is considered that the environment does not change substantially. There-
 665 fore, the predator–prey model must only be turned on when the conditions for deep con-
 666 vection onset are met and turned off after deep convection fully develops. Moreover, as
 667 shown in Section 3.2, the predator–prey system can be further generalized, to predict
 668 the convective fractional area at every vertical level of the numerical model. Future re-
 669 search is required to find the most appropriate predator–prey system for the shallow–
 670 to–deep transition and to tune the various coefficients introduced by the model.

671 As another very important contribution of the present conceptual model, a unified
 672 convection–cloud picture is described in which both clouds and convective elements in-
 673 teract with each other. Thus, the present predator–prey model also provides a param-
 674 eterization for the total cumulus fraction, a problem notorious for the climate projec-
 675 tions (e.g., Vogel et al., 2022). In addition, a complete unified parameterization might
 676 be built based on the principles introduced here by considering the prognostic Equation
 677 5 for the cloud fraction, and a bulk plume model that considers the local precondition-
 678 ing, as proposed for example by Vraciu et al. (2023). In the Vraciu et al. (2023) bulk plume
 679 model, a closure for the fraction of cloudy air entrained by the updrafts is required. How-
 680 ever, based on the predator–prey model described here, it might be considered that the
 681 predators are those updrafts that only entrain moist cloudy air, obtaining thus the frac-
 682 tion as the ratio between the predators and the prey. Furthermore, note that by con-
 683 sidering Equation 5, the boundary layer control of deep convection is implicit, in con-
 684 trast with the traditional mass–flux formulation in which a boundary layer control, al-
 685 though considered by many modern parameterizations, might be in fact inconsistent with
 686 the steady–state plume model of the mass–flux formulation (please refer to Yano et al.
 687 (2013) for a detailed discussion of this issue). Such a development is not presented here
 688 but left for future work.

689 Open Research

690 The LES data presented in Sections 3.1 and 3.2 of this work are openly available
 691 at Savre (2023a), while the data presented in Section 3.3 are available at Savre (2023b).
 692 The data presented in Figure 12 are openly available at Haerter (2021).

693 Acknowledgments

694 The authors thank Robert Plant for insightful comments and feedback. CVV ac-
 695 knowledges financial support from the Romanian Ministry of Research, Innovation, and
 696 Digitization through Project PN 23 21 01 01 and from the Romanian Ministry of Ed-
 697 ucation consisting in a doctoral scholarship received through the Doctoral School of Physics
 698 of the University of Bucharest.

699 References

700 Albright, A. L., Bony, S., Stevens, B., & Vogel, R. (2022). Observed subcloud-layer

- 701 moisture and heat budgets in the trades. *Journal of the Atmospheric Sciences*,
702 79(9), 2363–2385.
- 703 Albright, A. L., Stevens, B., Bony, S., & Vogel, R. (2023). A new conceptual picture
704 of the trade wind transition layer. *Journal of the Atmospheric Sciences*, 80(6),
705 1547–1563.
- 706 Arakawa, A. (2004). The cumulus parameterization problem: Past, present, and fu-
707 ture. *Journal of Climate*, 17(13), 2493–2525.
- 708 Arakawa, A., & Schubert, W. H. (1974). Interaction of a cumulus cloud ensemble
709 with the large-scale environment, Part I. *Journal of the Atmospheric Sciences*,
710 31(3), 674–701.
- 711 Bechtold, P., Bazile, E., Guichard, F., Mascart, P., & Richard, E. (2001). A mass-
712 flux convection scheme for regional and global models. *Quarterly Journal of*
713 *the Royal Meteorological Society*, 127(573), 869–886.
- 714 Bechtold, P., Chaboureaud, J.-P., Beljaars, A., Betts, A., Köhler, M., Miller, M., &
715 Redelsperger, J.-L. (2004). The simulation of the diurnal cycle of convective
716 precipitation over land in a global model. *Quarterly Journal of the Royal*
717 *Meteorological Society*, 130(604), 3119–3137.
- 718 Bechtold, P., Semane, N., Lopez, P., Chaboureaud, J.-P., Beljaars, A., & Bormann, N.
719 (2014). Representing equilibrium and nonequilibrium convection in large-scale
720 models. *Journal of the Atmospheric Sciences*, 71(2), 734–753.
- 721 Betts, A. K. (1976). Modeling subcloud layer structure and interaction with a shal-
722 low cumulus layer. *Journal of the Atmospheric Sciences*, 33(12), 2363–2382.
- 723 Böing, S. J., Jonker, H. J. J., Siebesma, A. P., & Grabowski, W. W. (2012).
724 Influence of the subcloud layer on the development of a deep convective
725 ensemble. *Journal of the Atmospheric Sciences*, 69, 2682–2698. doi:
726 10.1175/JAS-D-11-0317.1
- 727 Bretherton, C. S., McCaa, J. R., & Grenier, H. (2004). A new parameterization for
728 shallow cumulus convection and its application to marine subtropical cloud-
729 topped boundary layers. Part I: Description and 1D results. *Monthly Weather*
730 *Review*, 132(4), 864–882.
- 731 Champouillon, A., Rio, C., & Couvreux, F. (2023). Simulating the transition from
732 shallow to deep convection across scales: The role of congestus clouds. *Journal*
733 *of the Atmospheric Sciences*, 80(12), 2989–3005.
- 734 Christopoulos, C., & Schneider, T. (2021). Assessing biases and climate implications
735 of the diurnal precipitation cycle in climate models. *Geophysical Research Let-*
736 *ters*, 48(13), e2021GL093017.
- 737 Colin, M., Sherwood, S., Geoffroy, O., Bony, S., & Fuchs, D. (2019). Identifying the
738 sources of convective memory in cloud-resolving simulations. *Journal of the At-*
739 *mospheric Sciences*, 76(3), 947–962.
- 740 Colin, M., & Sherwood, S. C. (2021). Atmospheric convection as an unstable
741 predator–prey process with memory. *Journal of the Atmospheric Sciences*,
742 78(11), 3781–3797.
- 743 Couvreux, F., Roehrig, R., Rio, C., Lefebvre, M.-P., Komori, T., Derbyshire, S., ...
744 others (2015). Representation of daytime moist convection over the semi-
745 arid tropics by parametrizations used in climate and meteorological models.
746 *Quarterly Journal of the Royal Meteorological Society*, 141(691), 2220–2236.
- 747 Daleu, C. L., Plant, R., Woolnough, S., Stirling, A., & Harvey, N. (2020). Memory
748 properties in cloud-resolving simulations of the diurnal cycle of deep convec-
749 tion. *Journal of Advances in Modeling Earth Systems*, 12(8), e2019MS001897.
- 750 Damiani, R., Vali, G., & Haimov, S. (2006). The structure of thermals in cumu-
751 lus from airborne dual-Doppler radar observations. *Journal of the Atmospheric*
752 *Sciences*, 63(5), 1432–1450.
- 753 Davies, L., Plant, R., & Derbyshire, S. (2013). Departures from convective equi-
754 librium with a rapidly varying surface forcing. *Quarterly Journal of the Royal*
755 *Meteorological Society*, 139(676), 1731–1746.

- 756 Donner, L. J. (1993). A cumulus parameterization including mass fluxes, vertical
757 momentum dynamics, and mesoscale effects. *Journal of the Atmospheric Sci-*
758 *ences*, 50(6), 889–906.
- 759 Donner, L. J., & Phillips, V. T. (2003). Boundary layer control on convective avail-
760 able potential energy: Implications for cumulus parameterization. *Journal of*
761 *Geophysical Research: Atmospheres*, 108(D22), 4701.
- 762 Emanuel, K. A. (1991). A scheme for representing cumulus convection in large-scale
763 models. *Journal of the Atmospheric Sciences*, 48(21), 2313–2329.
- 764 Emanuel, K. A. (1993). A cumulus representation based on the episodic mixing
765 model: the importance of mixing and microphysics in predicting humidity. In
766 *The representation of cumulus convection in numerical models* (pp. 185–192).
767 Springer.
- 768 Grabowski, W. (2023). Daytime convective development over land: The role of sur-
769 face forcing. *Quarterly Journal of the Royal Meteorological Society*, 149(756),
770 2800–2819.
- 771 Grabowski, W., Bechtold, P., Cheng, A., Forbes, R., et al. (2006). Daytime con-
772 vective development over land: A model intercomparison based on LBA ob-
773 servations. *Quarterly Journal of the Royal Meteorological Society*, 132(615),
774 317–344.
- 775 Haerter, J. O. (2021). 1D (time) and 2D (time and vertical coordinate) data for the
776 cases DIU-500m, RCE-500m and DIU2RCE-500m [Data set]. *Zenodo*. doi:
777 <https://doi.org/10.5281/zenodo.4898182>
- 778 Harrington, E. L. (1958). Observations on the appearance and growth of tropical cu-
779 muli. *Journal of the Atmospheric Sciences*, 15(2), 127–130.
- 780 Harvey, N. J., Daleu, C. L., Stratton, R. A., Plant, R. S., Woolnough, S. J., & Stir-
781 ling, A. J. (2022). The impact of surface heterogeneity on the diurnal cycle
782 of deep convection. *Quarterly Journal of the Royal Meteorological Society*,
783 148(749), 3509–3527.
- 784 Hernandez-Deckers, D., & Sherwood, S. C. (2016). A numerical investigation of cu-
785 mulus thermals. *Journal of the Atmospheric Sciences*, 73(10), 4117–4136.
- 786 Heus, T., Jonker, H. J. J., Van den Akker, H. E., Griffith, E. J., Koutek, M., & Post,
787 F. H. (2009). A statistical approach to the life cycle analysis of cumulus clouds
788 selected in a virtual reality environment. *Journal of Geophysical Research:*
789 *Atmospheres*, 114(D6).
- 790 Hohenegger, C., & Bretherton, C. S. (2011). Simulating deep convection with a shal-
791 low convection scheme. *Atmospheric Chemistry and Physics*, 11(20), 10389–
792 10406.
- 793 Hohenegger, C., & Stevens, B. (2013). Preconditioning deep convection with cumu-
794 lus congestus. *Journal of the Atmospheric Sciences*, 70(2), 448–464.
- 795 Holloway, C. E., & Neelin, J. D. (2009). Moisture vertical structure, column wa-
796 ter vapor, and tropical deep convection. *Journal of the Atmospheric Sciences*,
797 66(6), 1665–1683.
- 798 Hwong, Y.-L., Colin, M., Aglas-Leitner, P., Muller, C. J., & Sherwood, S. C. (2023).
799 Assessing memory in convection schemes using idealized tests. *Journal of Ad-*
800 *vances in Modeling Earth Systems*, 15(12), e2023MS003726.
- 801 Jensen, G. G., Fiévet, R., & Haerter, J. O. (2022). The diurnal path to persistent
802 convective self-aggregation. *Journal of Advances in Modeling Earth Systems*,
803 14(5), e2021MS002923.
- 804 Jones, T. R., & Randall, D. A. (2011). Quantifying the limits of convective parame-
805 terizations. *Journal of Geophysical Research: Atmospheres*, 116(D8).
- 806 Kain, J. S., & Fritsch, J. M. (1993). Convective parameterization for mesoscale mod-
807 els: The Kain-Fritsch scheme. In *The representation of cumulus convection in*
808 *numerical models* (pp. 165–170). Springer.
- 809 Khairoutdinov, M., & Randall, D. (2006). High-resolution simulation of shallow-
810 to-deep convection transition over land. *Journal of the Atmospheric Sciences*,

- 811 63(12), 3421–3436.
- 812 Kjoenbongarit. (2013). *Forming cumulonimbus (timelapse)*. [https://www.youtube](https://www.youtube.com/watch?v=232LFz-aiz4)
- 813 [.com/watch?v=232LFz-aiz4](https://www.youtube.com/watch?v=232LFz-aiz4). YouTube. (Accessed: 21.07.2023)
- 814 Koenig, L. R. (1963). The glaciating behavior of small cumulonimbus clouds. *Journal of Atmospheric Sciences*, 20(1), 29–47.
- 815
- 816 Koren, I., & Feingold, G. (2011). Aerosol–cloud–precipitation system as a predator–prey problem. *Proceedings of the National Academy of Sciences of the United States of America*, 108(30), 12227–12232.
- 817
- 818
- 819 Kurowski, M. J., Suselj, K., Grabowski, W. W., & Teixeira, J. (2018). Shallow-to-deep transition of continental moist convection: Cold pools, surface fluxes, and mesoscale organization. *Journal of the Atmospheric Sciences*, 75(12), 4071–4090.
- 820
- 821
- 822
- 823 Malkus, J. S., & Scorer, R. S. (1955). The erosion of cumulus towers. *Journal of the Atmospheric Sciences*, 12, 43–57.
- 824
- 825 Markowski, P., & Richardson, Y. (2011). *Mesoscale meteorology in midlatitudes*. John Wiley & Sons.
- 826
- 827 Meyer, B., & Haerter, J. O. (2020). Mechanical forcing of convection by cold pools: Collisions and energy scaling. *Journal of Advances in Modeling Earth Systems*, 12(11), e2020MS002281.
- 828
- 829
- 830 Moorthi, S., & Suarez, M. J. (1992). Relaxed arakawa-schubert. a parameterization of moist convection for general circulation models. *Monthly Weather Review*, 120(6), 978–1002.
- 831
- 832
- 833 Morrison, H. (2017). An analytic description of the structure and evolution of growing deep cumulus updrafts. *Journal of the Atmospheric Sciences*, 74(3), 809–834.
- 834
- 835
- 836 Morrison, H., Peters, J. M., Chandrakar, K. K., & Sherwood, S. C. (2022). Influences of environmental relative humidity and horizontal scale of subcloud ascent on deep convective initiation. *Journal of the Atmospheric Sciences*, 79(2), 337–359.
- 837
- 838
- 839
- 840 Morrison, H., Peters, J. M., Varble, A. C., Hannah, W. M., & Giangrande, S. E. (2020). Thermal chains and entrainment in cumulus updrafts. Part I: Theoretical description. *Journal of the Atmospheric Sciences*, 77(11), 3637–3660.
- 841
- 842
- 843 Moser, D. H., & Lasher-Trapp, S. (2017). The influence of successive thermals on entrainment and dilution in a simulated cumulus congestus. *Journal of the Atmospheric Sciences*, 74(2), 375–392.
- 844
- 845
- 846 Neggers, R., Stevens, B., & Neelin, J. D. (2006). A simple equilibrium model for shallow-cumulus-topped mixed layers. *Theoretical and Computational Fluid Dynamics*, 20(5), 305–322.
- 847
- 848
- 849 Nelson, T. C., Marquis, J., Varble, A., & Friedrich, K. (2021). Radiosonde observations of environments supporting deep moist convection initiation during RELAMPAGO-CACTI. *Monthly Weather Review*, 149(1), 289–309.
- 850
- 851
- 852 Pan, D.-M., & Randall, D. D. (1998). A cumulus parameterization with a prognostic closure. *Quarterly Journal of the Royal Meteorological Society*, 124(547), 949–981.
- 853
- 854
- 855 Peters, J. M., Hannah, W., & Morrison, H. (2019). The influence of vertical wind shear on moist thermals. *Journal of the Atmospheric Sciences*, 76(6), 1645–1659.
- 856
- 857
- 858 Peters, J. M., Morrison, H., Nelson, T. C., Marquis, J. N., Mulholland, J. P., & Nowotarski, C. J. (2022). The influence of shear on deep convection initiation. Part I: Theory. *Journal of the Atmospheric Sciences*, 79(6), 1669–1690.
- 859
- 860
- 861 Pinsky, M., Eytan, E., Koren, I., & Khain, A. (2022). Convective and turbulent motions in nonprecipitating Cu. Part II: LES simulated cloud represented by a starting plume. *Journal of the Atmospheric Sciences*, 79(3), 793–813.
- 862
- 863
- 864 Plant, R. (2010). A review of the theoretical basis for bulk mass flux convective parameterization. *Atmospheric Chemistry and Physics*, 10(8), 3529–3544.
- 865

- 866 Powell, S. W. (2022). Criticality in the shallow-to-deep transition of simulated
867 tropical marine convection. *Journal of the Atmospheric Sciences*, *79*(7), 1805–
868 1819.
- 869 Raymond, D. J., & Blyth, A. M. (1989). Precipitation development in a New
870 Mexico thunderstorm. *Quarterly Journal of the Royal Meteorological Society*,
871 *115*(490), 1397–1423.
- 872 Rio, C., Del Genio, A. D., & Hourdin, F. (2019). Ongoing breakthroughs in convective
873 parameterization. *Current Climate Change Reports*, *5*, 95–111.
- 874 Rio, C., Grandpeix, J.-Y., Hourdin, F., Guichard, F., Couvreux, F., Lafore, J.-P., ...
875 others (2013). Control of deep convection by sub-cloud lifting processes: the
876 ALP closure in the LMDZ5B general circulation model. *Climate dynamics*, *40*,
877 2271–2292.
- 878 Rio, C., Hourdin, F., Grandpeix, J.-Y., & Lafore, J.-P. (2009). Shifting the diurnal
879 cycle of parameterized deep convection over land. *Geophysical Research Letters*,
880 *36*(7).
- 881 Rochetin, N., Couvreux, F., Grandpeix, J.-Y., & Rio, C. (2014). Deep convection
882 triggering by boundary layer thermals. Part I: LES analysis and stochastic
883 triggering formulation. *Journal of the Atmospheric Sciences*, *71*(2), 496–514.
- 884 Sakradzija, M., Seifert, A., & Heus, T. (2015). Fluctuations in a quasi-stationary
885 shallow cumulus cloud ensemble. *Nonlinear Processes in Geophysics*, *22*(1),
886 65–85.
- 887 Savre, J. (2023a). Outputs from new LBA simulations. Part I: Baseline case [Data
888 set]. *Zenodo*. doi: <https://doi.org/10.5281/zenodo.10409139>
- 889 Savre, J. (2023b). Outputs from new LBA simulations. Part III: Suppressed cold
890 pools [Data set]. *Zenodo*. doi: <https://doi.org/10.5281/zenodo.10417550>
- 891 Savre, J., & Craig, G. (2023). Fitting cumulus cloud size distributions from idealized
892 cloud resolving model simulations. *Journal of Advances in Modeling Earth Sys-*
893 *tems*, *15*(5), e2022MS003360.
- 894 Savre, J., Ekman, A. M. L., & Svensson, G. (2014). Technical note: Introduction
895 to MIMICA, a large-eddy simulation solver for cloudy planetary boundary
896 layers. *Journal of Advances in Modeling Earth Systems*, *6*, 630–649. doi:
897 10.1002/2013MS000292
- 898 Schiro, K. A., & Neelin, J. D. (2019). Deep convective organization, moisture ver-
899 tical structure, and convective transition using deep-inflow mixing. *Journal of*
900 *the Atmospheric Sciences*, *76*(4), 965–987.
- 901 Schlemmer, L., & Hohenegger, C. (2014). The formation of wider and deeper clouds
902 as a result of cold-pool dynamics. *Journal of the Atmospheric Sciences*, *71*(8),
903 2842–2858.
- 904 Scorer, R., & Ludlam, F. (1953). Bubble theory of penetrative convection. *Quarterly*
905 *Journal of the Royal Meteorological Society*, *79*(339), 94–103.
- 906 Sherwood, S. C., Hernández-Deckers, D., Colin, M., & Robinson, F. (2013). Slippery
907 thermals and the cumulus entrainment paradox. *Journal of the Atmospheric*
908 *Sciences*, *70*(8), 2426–2442.
- 909 Strong, M. (2017). *Time lapse of rising cumulus congestus III – rising turrets with*
910 *pileus*. <https://www.youtube.com/watch?app=desktop&v=2rHqVFu1m6w>.
911 YouTube. (Accessed: 16.10.2023)
- 912 Suselj, K., Kurowski, M. J., & Teixeira, J. (2019). A unified eddy-diffusivity/mass-
913 flux approach for modeling atmospheric convection. *Journal of the Atmo-*
914 *spheric Sciences*, *76*(8), 2505–2537.
- 915 Takeuchi, Y. (1996). *Global dynamical properties of lotka-volterra systems*. World
916 Scientific.
- 917 Tao, C., Xie, S., Ma, H.-Y., Bechtold, P., Cui, Z., Vaillancourt, P. A., ... others
918 (2023). Diurnal cycle of precipitation over the tropics and central United
919 States: intercomparison of general circulation models. *Quarterly Journal of the*
920 *Royal Meteorological Society*. doi: 10.1002/qj.4629

- 921 Tian, Y., Zhang, Y., Klein, S. A., & Schumacher, C. (2021). Interpreting the diurnal
 922 cycle of clouds and precipitation in the ARM GoAmazon observations: Shallow
 923 to deep convection transition. *Journal of Geophysical Research: Atmospheres*,
 924 *126*(5), e2020JD033766.
- 925 Torri, G., Kuang, Z., & Tian, Y. (2015). Mechanisms for convection triggering by
 926 cold pools. *Geophysical Research Letters*, *42*(6), 1943–1950.
- 927 Vogel, R., Albright, A. L., Vial, J., George, G., Stevens, B., & Bony, S. (2022).
 928 Strong cloud–circulation coupling explains weak trade cumulus feedback. *Nature*,
 929 *612*(7941), 696–700.
- 930 Vraciu, C. V., Kruse, I. L., & Haerter, J. O. (2023). The role of passive cloud vol-
 931 umes in the transition from shallow to deep atmospheric convection. *Geophysical*
 932 *Research Letters*, *50*(23), e2023GL105996.
- 933 Wagner, T. M., & Graf, H.-F. (2010). An ensemble cumulus convection parame-
 934 terization with explicit cloud treatment. *Journal of the Atmospheric Sciences*,
 935 *67*(12), 3854–3869.
- 936 Waite, M. L., & Khouider, B. (2010). The deepening of tropical convection by
 937 congestus preconditioning. *Journal of the Atmospheric Sciences*, *67*(8), 2601–
 938 2615.
- 939 Yano, J.-I. (2014). Formulation structure of the mass-flux convection parameteriza-
 940 tion. *Dynamics of Atmospheres and Oceans*, *67*, 1–28.
- 941 Yano, J.-I., Bister, M., Fuchs, Z., Gerard, L., Phillips, V., Barkidija, S., & Piriou,
 942 J.-M. (2013). Phenomenology of convection-parameterization closure. *Atmo-*
 943 *spheric Chemistry and Physics*, *13*(8), 4111–4131.
- 944 Yano, J.-I., & Plant, R. (2012a). Finite departure from convective quasi-equilibrium:
 945 Periodic cycle and discharge–recharge mechanism. *Quarterly Journal of the*
 946 *Royal Meteorological Society*, *138*(664), 626–637.
- 947 Yano, J.-I., & Plant, R. S. (2012b). Interactions between shallow and deep convec-
 948 tion under a finite departure from convective quasi equilibrium. *Journal of the*
 949 *Atmospheric Sciences*, *69*(12), 3463–3470.
- 950 Zhao, M., & Austin, P. H. (2005). Life cycle of numerically simulated shallow cu-
 951 mulus clouds. Part II: Mixing dynamics. *Journal of the Atmospheric Sciences*,
 952 *62*(5), 1291–1310.
- 953 Zhuang, Y., Fu, R., Marengo, J. A., & Wang, H. (2017). Seasonal variation of
 954 shallow-to-deep convection transition and its link to the environmental con-
 955 ditions over the Central Amazon. *Journal of Geophysical Research: Atmo-*
 956 *spheres*, *122*(5), 2649–2666.

The rapid transition from shallow to precipitating convection as a predator–prey process

Cristian V. Vraciu^{1,2}, Julien Savre³, Maxime Colin⁴

¹Faculty of Physics, University of Bucharest, Bucharest–Măgurele, Romania

²Department of Theoretical Physics, Horia Hulubei National Institute of Physics and Nuclear Engineering, Măgurele, Romania

³Meteorology Institute, Ludwig-Maximilians-Universität München, Munich, Germany

⁴Leibniz Centre for Tropical Marine Research, Bremen, Germany

Key Points:

- A conceptual picture for cumulus cloud populations based on cloud–updraft interaction is discussed
- The local shallow preconditioning and the cold pool feedback imply a predator–prey type of interaction in the cloud–precipitation system
- A simple predator–prey model shows good agreement with idealized numerical simulations for the rapid shallow–to–deep transition.

Corresponding author: Cristian V. Vraciu, cristian.vraciu@theory.nipne.ro

16 Abstract

17 Properly predicting the rapid transition from shallow to precipitating atmospheric con-
 18 vection within a diurnal cycle over land is of great importance for both weather predic-
 19 tion and climate projections. In this work, we consider that a cumulus cloud is formed
 20 due to the transport of water mass by multiple updrafts during its life-time. Cumulus
 21 clouds then locally create favorable conditions for the subsequent convective updrafts
 22 to reach higher altitudes, leading to deeper precipitating convection. This mechanism
 23 is amplified by the cold pools formed by the evaporation of precipitation in the sub-cloud
 24 layer. Based on this conceptual view of cloud-cloud interactions which goes beyond the
 25 one cloud equals one-plume picture, it is argued that precipitating clouds may act as preda-
 26 tors that prey on the total cloud population, such that the rapid shallow-to-deep tran-
 27 sition can be modeled as a simple predator-prey system. This conceptual model is val-
 28 idated by comparing solutions of the Lotka-Volterra system of equations to results ob-
 29 tained using a high-resolution large-eddy Simulation model. Moreover, we argue that the
 30 complete diurnal cycle of deep convection can be seen as a predator-prey system with
 31 varying food supply for the prey. Finally, we suggest that the present model can be ap-
 32 plied to weather and climate models, which may lead to improved representations of the
 33 transition from shallow to precipitating continental convection.

34 Plain Language Summary

35 The rapid transition from shallow to precipitating convection over land is still poorly rep-
 36 resented by weather and climate models. In this work, we argue that this is due to the
 37 fact that the convective parameterization schemes only consider the interaction between
 38 the clouds and their environment, which is a slow process, and do not consider cloud-
 39 cloud interactions during the transition, which is a fast process. We show that this lat-
 40 ter interaction can be modeled as a predator-prey process, and we show how a very sim-
 41 ple dynamical model for cloud population can lead to improved prediction for the pre-
 42 cipitation rate and cloud cover over land.

43 1 Introduction

44 Atmospheric convection transports heat and moisture from the surface throughout the
 45 troposphere creating cumulus and cumulonimbus clouds that are responsible for the wa-
 46 ter cycle in the atmosphere and have a strong radiative forcing that can lead to either
 47 warming or cooling of the atmosphere. Shallow cumulus clouds are non-precipitating,
 48 or weakly precipitating convective clouds that form when the updraft plumes from the
 49 boundary layer reach the lifting condensation level but are unable to reach higher alti-
 50 tudes as they lose their buoyancy very quickly. Predicting shallow clouds is very impor-
 51 tant for climate predictability as they cover a very large part of the Earth and have a
 52 strong cooling effect on the climate system since they reflect an important fraction of
 53 the solar radiation back into space. When the atmosphere is unstable and the updraft
 54 plumes are able to reach the level of free convection, deep, precipitating convection is
 55 initiated. The deep convective clouds (congestus and cumulonimbus) precipitate, and
 56 re-stabilize the atmosphere as they warm and dry their environment. Since the cumu-
 57 lonimbus clouds are responsible for the formation of cirrus clouds, they also play a very
 58 important role in controlling the radiative budget of the Earth, as the cirrus clouds have
 59 a net warming effect. Therefore, the manner shallow and deep convective clouds are rep-
 60 resented in climate models has a significant impact on climate predictions.

61 In general, the presence of a convective inhibition (CIN) layer prevents boundary
 62 layer updrafts from spontaneously reaching their level of free convection and slows down
 63 the development of deep precipitating clouds: in this situation, shallow cumuli develop
 64 first and contribute to the creation of conditions favorable to deep convection. The tran-

sition from shallow to precipitating convection can be considered of two types: (i) a slow transition when at the beginning the atmosphere is not unstable enough to sustain the development of precipitating convection, and the shallow cumuli slowly moisten the atmosphere until the environment is unstable enough to allow the clouds to grow deeper and precipitate (Yano & Plant, 2012b; Champouillon et al., 2023), which is a process that takes typically a few days; (ii) a rapid transition in which the atmosphere is already unstable but deep precipitating convection still takes a few hours to develop. This rapid transition occurs usually over the tropics where the atmosphere is always unstable (Hohenegger & Stevens, 2013). In a diurnal cycle over land, the rapid transition has been documented by several authors (Grabowski et al., 2006; Khairoutdinov & Randall, 2006; Kurowski et al., 2018; Grabowski, 2023; Savre & Craig, 2023). In this particular case, the transition starts when the convective inhibition becomes small, and it takes around 3-4 hours for precipitation to properly develop, despite having a very large convective available potential energy (CAPE) from the beginning. In this study, we focus on the second kind of shallow-to-deep transition.

Although in recent years many studies investigated the physical processes controlling the rapid transition from shallow to precipitating convection (Kurowski et al., 2018; Peters et al., 2022; Powell, 2022; Rochetin et al., 2014; Schiro & Neelin, 2019), weather and climate models still predict the onset of deep precipitating convection to occur around 2-5 hours earlier when compared to observations (Christopoulos & Schneider, 2021) or large-eddy simulation (LES) (Bechtold et al., 2004; Grabowski et al., 2006; Couvreux et al., 2015; Harvey et al., 2022; Tao et al., 2023) within a diurnal cycle over land. That is because the convective parameterization schemes immediately switch to deep convection when CIN is very small and CAPE is large, although in reality, even when these conditions are met, the transition still takes a few hours, or may not even occur within a diurnal cycle (Khairoutdinov & Randall, 2006; Nelson et al., 2021; Tian et al., 2021; Zhuang et al., 2017).

The majority of convective parameterization schemes used in climate models are based on the so-called mass-flux parameterization. The objective of these parameterizations is to find the mass flux of the clouds and to provide feedback to the large-scale resolved by the model. The mass-flux formulation is based on the idea that the clouds, or the whole ensemble of clouds, can be modeled as steady-state plumes. In the picture used by these formulations, a convective cloud is formed by only one entraining plume, which only entrains environmental air described by the mean resolved state (Arakawa, 2004; Plant, 2010; Yano, 2014). Thus, the mass flux is estimated in these parameterization schemes only by considering the large-scale state, neglecting any cloud-cloud interaction or heterogeneity within a given grid box. As the mass flux only changes with the slow change of the large-scale state, these schemes are unable to catch any rapid transition from shallow to precipitating convection (Bechtold et al., 2004). At the time Arakawa and Schubert (1974) formulated their parameterization, the grid box and the time-stepping used by climate models were so large that over the tropical ocean one could consider that at all times within a grid-box there is a spectrum of shallow and precipitating clouds that are in quasi-equilibrium with their environment. Many operational parameterization schemes still follow the original mass-flux formulation introduced by Arakawa and Schubert (1974) (e.g., Bechtold et al., 2014; Kain & Fritsch, 1993; Rio et al., 2019). However, nowadays, climate models have much finer resolutions, both in space and time, and the quasi-equilibrium is therefore not satisfied in every grid box at every time step (Davies et al., 2013; Donner & Phillips, 2003; Jones & Randall, 2011). To improve the representation of atmospheric convection in numerical models with high temporal resolution, several prognostic closures for the convective mass flux with relaxed quasi-equilibrium have later been formulated (e.g., Moorthi & Suarez, 1992; Pan & Randall, 1998; Wagner & Graf, 2010; Yano & Plant, 2012a)

117 In general, the time evolution of the convective mass flux at cloud base M_c can be
 118 written as:

$$\frac{dM_c}{dt} = \rho_0 \sigma_c \frac{dw_c}{dt} + \rho_0 w_c \frac{d\sigma_c}{dt}, \quad (1)$$

119 where t is the time, ρ_0 is the atmospheric density at the cloud base, σ_c is the convective
 120 cloud cover, and w_c is the convective updraft velocity of the convective clouds. The mass-
 121 flux parameterizations usually consider that σ_c is constant, and thus, only the first term
 122 on the right hand side (rhs) of Equation 1 is important. Although the traditional mass-
 123 flux formulations do not make the assumption that σ_c is constant in an explicit way, such
 124 an assumption can be easily justified if the grid box and the time step are very large,
 125 such that the fluctuations in σ_c are subgrid, and the increase in cloud population in a
 126 small subdomain is compensated by the decay of clouds in another small subdomain. There-
 127 fore, in the mass-flux parameterization schemes, the triggering of individual convective
 128 clouds is not considered, but rather the whole spectrum of clouds that slowly interacts
 129 with the large-scale environment (Yano et al., 2013). It should also be noted that pa-
 130 rameterization models that implement a momentum equation for w_c have been formu-
 131 lated (e.g., Donner, 1993; Bechtold et al., 2001; Bretherton et al., 2004), in which the
 132 assumption that σ_c is constant is made in an explicit way. As in the original mass-flux
 133 formulation based on quasi-equilibrium, the prognostic formulations of Pan and Ran-
 134 dall (1998) and Wagner and Graf (2010) also consider a constant σ_c , and a steady-state
 135 plume that only interacts with a homogeneous environment. On the other hand, Yano
 136 and Plant (2012a, 2012b) assume that the time evolution of the mass flux is only con-
 137 trolled by the convective cloud cover, but it also considers the steady-state plume model
 138 while completely neglecting any cloud-cloud interaction.

139 Within a diurnal cycle over land, however, if the atmosphere is already unstable
 140 in the morning, the convection develops quite rapidly, while the cloud environment re-
 141 mains rather steady during the day (Tian et al., 2021). In such cases, one can no longer
 142 assume that the convection only interacts with the environment, and thus, convective
 143 memory might be important (Colin et al., 2019; Daleu et al., 2020; Colin & Sherwood,
 144 2021; Hwong et al., 2023). Although the above mentioned prognostic formulations also
 145 introduce convective memory into their formulation, this is achieved based on *ad-hoc*
 146 relations, and not based on physical considerations. The main assumption in these prog-
 147 nostic formulations is that M_c does not respond immediately to changes in the large-
 148 scale state. However, it is not clear why such an assumption might be true for a steady-
 149 state plume that only interacts with a homogeneous environment. In the present work,
 150 we assume that the updraft velocity at cloud base only exhibits a slow change during
 151 the rapid shallow-to-deep transition over land (e.g., Figure 15 of Kurowski et al., 2018),
 152 whereas the cloud fraction of the precipitating clouds evolves from zero in the morning
 153 to a maximum around noon, and thus, for this particular case, the second term in the
 154 rhs of Equation 1 becomes significant. Thus, the scope of this study is to find a dynam-
 155 ical system able to represent the evolution of σ_c during the rapid transition from shal-
 156 low to precipitating convection.

157 To predict the onset of deep precipitating convection, some numerical models as-
 158 sume CIN type triggering functions, which are used to turn on the deep convection scheme
 159 only if the updraft plumes in the boundary layer have a kinetic energy greater than CIN
 160 (Rio et al., 2009, 2013). However, such an implementation does not change the basis of
 161 the parameterization schemes but only decides when the scheme is active or not. If the
 162 scheme assumes a constant σ_c , then σ_c will jump from zero before triggering to a fixed
 163 value at triggering, remaining constant as long as the deep convective scheme is active.
 164 The problem with this kind of triggering function is that it does not allow for deep con-
 165 vection to properly develop from shallow convection, which results in predicting the on-
 166 set of precipitating convection several hours sooner. To ameliorate this problem, several

parameterization schemes assume that within a diurnal cycle, at the triggering, even if CAPE is very large, deep cumulonimbus clouds only form if cold pools are also present (e.g., Hohenegger & Bretherton, 2011; Suselj et al., 2019). However, since CAPE is already large at the triggering time, the convective scheme immediately creates precipitation, being unable to capture the transition from the non-precipitating shallow cumuli to the precipitating congestus clouds. Thus, they are unable to fully correct the time of precipitation onset, but keep the precipitation rate small until the cumulonimbus clouds develop. In this work, we propose a conceptual model for cumulus clouds that allow for a gradual evolution of σ_c when the triggering conditions are met, governed by a predator-prey-type dynamical system.

2 Conceptual Model

In our model the clouds are formed due to the transport of water by the updrafts from the boundary layer. In contrast with the mass-flux formulation, we do not consider that every cloud, or every cloud ensemble, is described by only one steady-state plume, but we consider that a cloud can be formed by the contribution of multiple unsteady convective elements — such as thermals (e.g., Scorer & Ludlam, 1953; Sherwood et al., 2013; Hernandez-Deckers & Sherwood, 2016) or starting plumes (Pinsky et al., 2022) — as also suggested by several authors (e.g., Malkus & Scorer, 1955; Moser & Lasher-Trapp, 2017; Morrison et al., 2020; Vraciu et al., 2023). Indeed, the pulsating behavior of clouds has been documented by both observational studies (e.g., Harrington, 1958; Koenig, 1963; Raymond & Blyth, 1989; Damiani et al., 2006) and numerical simulations (e.g., Zhao & Austin, 2005; Heus et al., 2009; Sakradzija et al., 2015; Peters et al., 2019), which may indicate the presence of successive convective elements within the clouds. Each convective element transports a finite mass of water from the boundary layer to the cloud layer, and the cloud dimension is given by the total amount of water transported by the set of convective elements that reach the condensation level in that given place of the cloud during its life-time, minus the amount of cloud water that evaporates due to mixing with the environment (detrainment). The episodic mixing model of Emanuel (1991) is in fact based on a very similar conceptual picture (see also Emanuel, 1993). Emanuel (1991) makes very clear that in his parameterization scheme, the small convective elements within the clouds are responsible for the convective transport: “I am explicitly attempting to represent the collective effects of an ensemble of individual, $\mathcal{O}(100\text{ m})$ -scale drafts, not of ensembles of $\mathcal{O}(1\text{ km})$ -scale clouds. These drafts, rather than whole clouds, are regarded as the fundamental agents of convective transport.” Thus, in this picture, a cloud can be seen as analogous to a wall of bricks, and a convective element as a new brick fixed on the wall by the builder — the clouds are seen as a collection of water elements brought by a number of convective elements during the cloud life-time, in which every water element represents a brick in our wall. This building process can be visualized for the development of a real cumulonimbus cloud at Kjoenbongarit (2013) or for a congestus cloud at Strong (2017).

We consider here two types of clouds: (i) nonprecipitating shallow cumuli, which are those clouds with a top close to the boundary layer depth, covering a fraction σ_s — this type of clouds remain shallow as they are unable to gain buoyancy, or lose their buoyancy very quickly; and (ii) convective precipitating clouds, which are clouds that are able to gain some buoyancy and have a top much deeper than the boundary layer depth, covering a fraction σ_c . Here, we consider that the convective precipitating clouds have a top above 4 km. Therefore, the total cloud cover is $\sigma = \sigma_s + \sigma_c$. We consider that the difference between the shallow and convective precipitating clouds is that the shallow clouds decay only due to mixing (detrainment) into the environment, whereas the convective precipitating clouds decay also by precipitation. Although the shallow cumuli can also lightly precipitate, we consider that the precipitation rate of shallow cumuli can be neglected with respect to the precipitation rate of convective precipitating clouds.

219 We consider that the total mass m_j of cloud j is given by:

$$m_j = \sum_i^n \delta m_i - m_{D,j}, \quad (2)$$

220 where δm_i is the mass transported into the cloud by the convective element i , n is the
 221 total number of convective elements that contribute to cloud j during its life-time, and
 222 $m_{D,j}$ is the mass lost by the cloud due to mixing with the dry environment and precip-
 223 itation. Here, by cloud mass, we refer to the mass of air within a cloud, but other quan-
 224 tities might be considered as well, such as the mass of condensed particles (water plus
 225 ice), or the total integrated condensed water path. For the whole ensemble of clouds we
 226 can write:

$$m = \sum_j m_j = \bar{\rho} \sigma \overline{\Delta z}, \quad (3)$$

227 where m and $\overline{\Delta z}$ are the total mass and the average depth of the cloud ensemble, respec-
 228 tively, and $\bar{\rho}$ is the mean air density within the clouds. Here, all masses are per unit of
 229 area, so the masses in Equation 2 have units of kg m^{-2} . For the evolution of m , neglect-
 230 ing the time change of $\bar{\rho}$, we thus have:

$$\frac{dm}{dt} = \bar{\rho} \sigma \frac{d\overline{\Delta z}}{dt} + \bar{\rho} \overline{\Delta z} \frac{d\sigma}{dt} = M_0 - D, \quad (4)$$

231 where M_0 is the sum of the contributions from all convective elements to the total mass
 232 flux at the condensation level and $D = d(\sum_j m_{D,j})/dt$, is the rate at which the cloud
 233 ensemble loses mass due to evaporation and precipitation. Therefore, the evolution of
 234 the cloud fraction becomes:

$$\frac{d\sigma}{dt} = \frac{M_0 - D}{\bar{\rho} \overline{\Delta z}} - \sigma \frac{d(\ln \overline{\Delta z})}{dt}. \quad (5)$$

235 For a shallow case at equilibrium, $M_0 - D = 0$, meaning that the new mass brought
 236 into the cloud layer by the convective elements is compensated by the detrainment into
 237 the environment. However, during the shallow-to-deep transition, $\overline{\Delta z}$ increases rapidly,
 238 and the second term in the rhs of Equation 5 is positive and contributes to a reduction
 239 of the total cloud cover. It should be noted that, during the transition, $M_0 - D$ may
 240 not be constant as for a shallow case at equilibrium, but we assume that the contribu-
 241 tion from this term remains generally small compared to the second term in the rhs of
 242 Equation 5. Besides, it is clear that since the first term on the rhs is inversely propor-
 243 tional to $\overline{\Delta z}$, the contribution from $M_0 - D$ to the evolution of σ will decrease as the
 244 cloud layer depth increases. Equation 5 thus indicates that the mass conservation implies
 245 a reduction in the total cloud fraction during the rapid shallow-to-deep transition.

246 2.1 Local Moisture Preconditioning

247 Because the moisture of the cloud environmental layer has been observed to be an im-
 248 portant factor in the transition from shallow to precipitating convection, some studies
 249 argue that the rapid transition from shallow to precipitating convection can be explained
 250 by the moistening of the cloud environment by the shallow cumuli (Holloway & Neelin,
 251 2009; Waite & Khouider, 2010), which is known as the moisture preconditioning mech-
 252 anism. This idea can be perhaps better understood if we consider the following plume
 253 model (Morrison, 2017):

$$\frac{dB}{dz} = -N^2 - \varepsilon B - \varepsilon \frac{gL_v q_{sE}(1 - \mathcal{R}_E)}{c_p T_E \Gamma}, \quad (6)$$

254 where B is the plume buoyancy, z is the vertical coordinate, N^2 is the squared buoyancy
 255 frequency, ε is the entrainment rate, g is the gravitational acceleration, L_v is the latent
 256 heat of vaporization, q_{sE} is the saturation mixing ratio of the environment, \mathcal{R}_E is the
 257 environmental relative humidity, T_E is the temperature of the environment, c_p is the spe-
 258 cific heat of air at constant pressure, and $\Gamma \approx 1 + L_v^2 q_{sE} / (c_p R_v T_E^2)$ is a parameter, for
 259 which R_v is the water vapor gas constant. The last term in the rhs of Equation 6 rep-
 260 represents the cooling rate of the updraft plume due to the evaporation of the cloud water
 261 that mixes with the dry environmental air. Thus, as shallow cumuli continue to increase
 262 RH_E , this term will continue to decrease, allowing the plumes to deepen the cloud layer
 263 (Morrison et al., 2022). However, Hohenegger and Stevens (2013) showed that the mois-
 264 ture preconditioning acts at time scales too long to explain the rapid transition. Note
 265 that the concept of preconditioning as formulated by Waite and Khouider (2010) or Yano
 266 and Plant (2012b) is based on the same consideration as the mass-flux formulation, with
 267 steady plumes that entrains air described by a mean domain value.

268 On the other hand, Vraciu et al. (2023) discussed the role of passive shallow cu-
 269 muli in the transition from shallow to deep convection, which can be regarded as local
 270 moisture preconditioning. As in the moisture preconditioning mechanism described by
 271 (e.g., Waite & Khouider, 2010), the idea is that if the updraft plumes can entrain moister
 272 air, they will be able to grow deeper due to a smaller contribution of the last term in the
 273 rhs of Equation 6. However, the main difference is that we no longer assume a steady-
 274 state plume that entrains air only described by a mean state, as in the mass-flux for-
 275 mulation, but we consider that the plumes (or any other convective elements) have a smaller
 276 life-time than the clouds, and are allowed to develop in the place of existing clouds. Thus,
 277 the cloud itself provides a local preconditioning for the development of the subsequent
 278 convective elements, as also shown by Moser and Lasher-Trapp (2017). This process of
 279 interaction between the convective elements and the existing clouds leads to deeper and
 280 deeper clouds. Furthermore, we can also consider that the clouds, even after a complete
 281 decay, still leave spots of abnormally large humidity that slowly dissipate into the en-
 282 vironment (e.g. Figure 7 of Daleu et al., 2020). Thus, if the convective elements reach
 283 the condensation level in the location of such spots, they will again benefit from the lo-
 284 cal preconditioning, creating deeper clouds. We may also consider that the area of these
 285 spots is proportional to the total cloud cover at the cloud base.

286 Let us consider that at a given time we have a cloud field of shallow cumuli, as schemat-
 287 ically presented in Figure 1A. We consider that every cloud, either shallow or deep, is
 288 formed by a set of convective elements that transported water from the boundary layer
 289 to the cloud layer. After a given time, a new set of convective elements reaches the con-
 290 densation level. Here, we have two possibilities: (i) the convective elements reach the con-
 291 densation level in a place where there are no clouds (or spots of large humidity), form-
 292 ing new shallow cumuli. This case is schematically illustrated in Figure 1B. At the same
 293 time, some of the clouds decay during the development of the new convective elements,
 294 and thus, we can consider that the new clouds statistically replace the old ones that died;
 295 (ii) the new set of convective elements reach the condensation level in the place of an al-
 296 ready existing cloud, as schematically illustrated in Figure 1C. In this case, the convec-
 297 tive elements will transport water from the boundary layer in a higher cloud layer, while
 298 some of the shallow clouds decay. As a result, the total cloud fraction σ decreases, while
 299 the fraction of clouds that become convective σ_c increases.

300 As convection becomes more intense, the compensating entrainment of dry air from
 301 the cloud layer into the boundary layer also increases, which creates a stable transition
 302 layer between the top of the boundary layer z_i and the lifting condensation level (LCL)
 303 (Betts, 1976; Neggers et al., 2006; Albright et al., 2022). As a result, the mass flux of

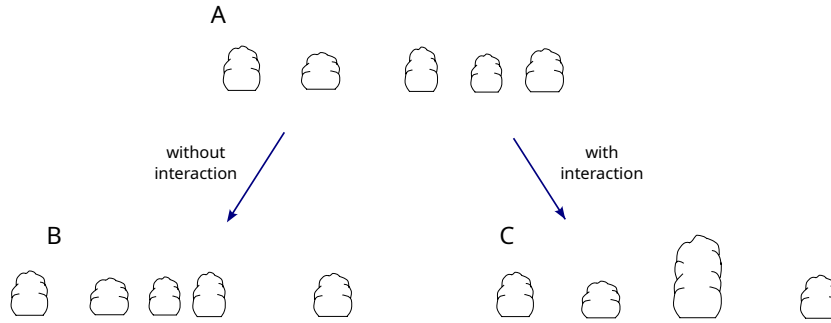


Figure 1. Deepening of a cumulus clouds due to local preconditioning. (A) initial cloud field with five shallow cumuli. (B) after a time, one of the clouds decays, while a new set of convective elements, that do not interact with the existing clouds, forms a new shallow cumulus. As a result, the cloud fraction remains steady. (C) as in (B), but now the new set of convective elements develop in the place of one of the existing clouds, forming a deeper, convective precipitating cloud. As a result, the cloud fraction at cloud base decreases, while the cloud fraction of convective precipitating cumuli increases.

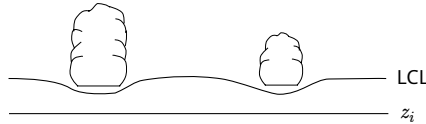


Figure 2. Schematics of non-precipitating clouds altering the transition layer between z_i and LCL.

304 the updrafts at cloud base may also decrease as the number of convective precipitating
 305 clouds increases. Because the non-precipitating clouds always mix with the environment
 306 due to diffusion and turbulent mixing, we expect the air just below the base of a given
 307 non-precipitating cloud to be moister than the air at the same height but in a cloud-
 308 less area (e.g. Albright et al., 2023). Thus, as the convective elements that develop in
 309 the place of an already existing cloud mix moister air than those developing in the cloud-
 310 less areas, we consider that the non-precipitating clouds also create heterogeneity in the
 311 stable transition layer (Figure 2), making easier for the convective elements to reach the
 312 condensation level where there are already non-precipitating clouds present. This altera-
 313 tion of the transition layer is also supported by the findings of Vraciu et al. (2023) who
 314 showed that the fraction of convective elements that develop where a cloud is already
 315 present is comparable with the fraction of convective elements that develop in cloudless
 316 areas, even though the clouds only occupy a very small fractional area. Therefore, we
 317 expect the fraction of updrafts at the cloud base to also decrease with the decrease of
 318 σ , which leads to a further reduction in σ . The local shallow preconditioning thus leads
 319 to deeper clouds, which due to mass conservation and alteration of the transition layer
 320 leads to a reduction in the cloud cover at cloud base.

321 2.2 Cold Pools Feedback

322 Once the clouds begin to precipitate, cold pools are formed in the boundary layer, which
 323 organize the convective field. This organization can be seen as updrafts being larger and
 324 more organized (Schlemmer & Hohenegger, 2014; Meyer & Haerter, 2020). This leads
 325 to further deepening of the cloud layer for two reasons: firstly, the larger convective el-

326 elements experience smaller entrainment (Kurowski et al., 2018; Schlemmer & Hohenegger,
 327 ger, 2014), and thus, are able to better preserve their buoyancy, and secondly, more or-
 328 ganized convective elements facilitate the local preconditioning, as the probability for
 329 a set of convective elements to develop in a certain place (to cluster) is larger. Although
 330 one may argue that the cold pools lead to convective elements that are so large that they
 331 do not require local preconditioning, Savre and Craig (2023) show that, during the tran-
 332 sition, the increase in the updraft dimension is negligible compared with the increase in
 333 cloud dimension — there are no updrafts as large as a deep convective cloud, and thus,
 334 we argue here that cold pools essentially make the local preconditioning more efficient
 335 without substantially altering the properties of the boundary layer updrafts. In other
 336 words, we still consider that a convective cloud is a result of multiple convective elements
 337 bringing water from the boundary layer in the same location, but since the convective
 338 elements are larger and better organized, a smaller number of convective elements are
 339 required to build a precipitating cloud. Following the analogy between clouds and brick
 340 walls, we can picture the cold pool feedback as having sets of bricks that are already tied
 341 together, and thus, the building process is much more efficient since the builder brings
 342 a new set of tied bricks with only one move. Although we do not consider that it is im-
 343 possible for only one convective element to create a precipitating cloud, we consider that
 344 even in this case, the convective element will benefit from the large humidity spots cre-
 345 ated by the non-precipitating clouds, and such a situation might rather correspond to
 346 the creation of “turkey towers” (e.g. Figure 7.14 in Markowski & Richardson, 2011), rather
 347 than the creation of congestus or cumulonimbus clouds.

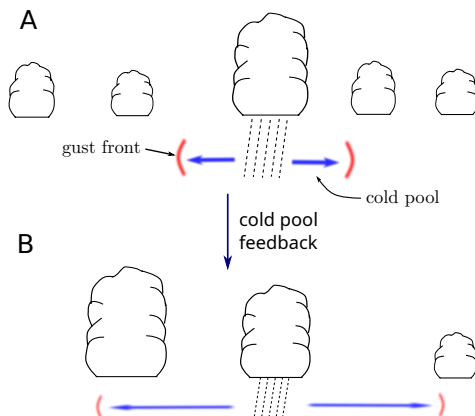


Figure 3. Deepening of a cumulus clouds due to cold pool feedback. (A) initial cloud field with four shallow clouds and one convective cloud in the decaying precipitating stage, which creates a cold pool that leads to the development of a new convective precipitating cloud at a later time (B). At the same time, some of the shallow clouds decay without being replaced by new shallow cumuli. As the precipitating clouds, being deeper, occupy a smaller fraction than the shallow cumuli, for the same amount of building convective elements, the total cloud cover decreases.

348 In Figure 3, we illustrate the effect of the cold pools in the deepening of subsequent
 349 convection. Initially, we consider a field of shallow and precipitating clouds. The pre-
 350 cipitating cloud illustrated in Figure 3A precipitates, creating a cold pool, and a new con-
 351 vective precipitating cloud is formed later on, as schematically illustrated in Figure 3B.
 352 Since the convective elements are larger and more organized, more water is transported
 353 by them to higher altitudes, which leads to a net decrease in the total cloud field. More-
 354 over, although the cold pools trigger new updrafts at their gust fronts (Torri et al., 2015;
 355 Meyer & Haerter, 2020), as the cold pools represent areas of evaporatively cooled down-

356 drafts they also inhibit updrafts from developing within these areas. The cold pools thus
 357 make the convective elements to be fewer but stronger (e.g. Figure 15 of Kurowski et
 358 al., 2018). Therefore, we also expect a reduction in the updraft fraction at the cloud base
 359 due to cold pool feedback.

360 2.3 Predator-Prey Model

361 The physical processes discussed above suggest that the transition from shallow to pre-
 362 cipitating convection can be modeled as a predator-prey process with convective precip-
 363 itating clouds acting as predators, and the total cloud field acting as prey. We consider
 364 that the prey is represented by the total cloud field as both the shallow and convective
 365 precipitating clouds precondition their local environment, as long as the convective pre-
 366 cipitating clouds are not in the decaying precipitating stage. However, we consider that
 367 the fraction of clouds in the decaying precipitating stage is much smaller than the total
 368 cloud fraction.

369 Here, for simplicity, we consider a very simple predator-prey model, namely the
 370 Lotka-Volterra model (Takeuchi, 1996), given by:

$$\frac{dx}{dt} = ax - bxy, \tag{7}$$

$$\frac{dy}{dt} = exy - fy, \tag{8}$$

371 where x is the population of prey and y is the population of predators, and a , b , e , and
 372 f are system coefficients. A solution of the Lotka-Volterra system is presented in Fig-
 373 ure 4.

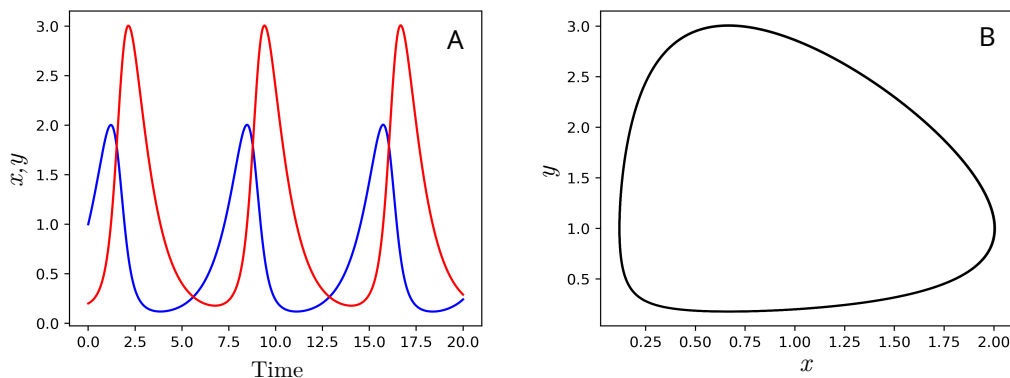


Figure 4. Solution of the Lotka-Volterra system. (A) Time evolution of prey (blue solid line) and predators (red solid line); (B) Limit cycle of the system.

374 In our case, we consider that the prey is played by the total cloud population at
 375 cloud base, which sustains the development of the deeper clouds, that act as predators.
 376 Thus, we consider $x = \sigma$ and $y = \sigma_c$. The first term in the rhs of Equation 7 repre-
 377 sents the difference between the source of new convective elements from the boundary
 378 layer and the decay of the old clouds due to the mixing with the environment and pre-
 379 cipitation. In the absence of precipitation, all the clouds are shallow. As shallow cumuli
 380 moisten their environment, we expect the shallow cloud cover to increase as the life-time

381 of the clouds increases due to mixing with moister and moister air. Thus, in the absence
 382 of precipitation, the shallow cloud cover grows exponentially, which might correspond
 383 to a cumulus-to-stratiform transition, rather than the case considered here. The sec-
 384 ond term represents the decay in the cloud cover due to interactions between precipi-
 385 tating clouds and the rest of the cloud population. σ_c appears in this term for two rea-
 386 sons: firstly, the deeper clouds have longer life-times and are wider, hence increasing the
 387 probability for new convective elements to interact with them, and secondly, when they
 388 precipitate, they form cold pools that trigger new precipitating clouds thus further de-
 389 creasing the total cloud cover (see Section 2.2). The first term on the rhs of Equation
 390 8 represents the growth of convective precipitating clouds for the same physical argu-
 391 ments as for the second rhs term of the prey equation. Lastly, the last term in the rhs
 392 of Equation 8 represents the decay rate of convective precipitating clouds due to precip-
 393 itation and dissipation into the environment. An important limitation of the Lotka-Volterra
 394 model, however, is that predators cannot be created from nothing, and thus, σ_c must be
 395 initialized with a nonzero value. Note that the predator-prey system described here com-
 396 prises cannibalism as the total cloud population, including precipitating clouds, acts as
 397 a prey for the precipitating cloud population.

398 Although more realistic and accurate predator-prey models may be considered here,
 399 the Lotka-Volterra model was selected for its simplicity. Besides, it should be kept in
 400 mind that the coefficients of the predator-prey system may not be universal, but may
 401 rather depend on other meteorological parameters, such as environmental relative hu-
 402 midity, or the boundary layer depth, which are well-known to be important parameters
 403 in the shallow-to-deep transition (e.g., Morrison et al., 2022; Grabowski, 2023).

404 Similar predator-prey models for the cloud-precipitation system have previously
 405 been formulated by Colin and Sherwood (2021) and Koren and Feingold (2011), but based
 406 on completely different physical arguments, and not for the specific transition case dis-
 407 cussed here. Our model also differs from the predator-prey model of Wagner and Graf
 408 (2010) where a Lotka-Volterra model was used to model interactions between cloud species,
 409 excluding cannibalism.

410 **3 Tests and Extensions of the Predator-Prey Model**

411 **3.1 LBA Transition Case**

412 Results obtained from a high-resolution large-eddy simulation (LES) were analysed in
 413 order to test our hypotheses. The model configuration constitutes an idealization of the
 414 original Large-scale Biosphere-Atmosphere (LBA) case described in Grabowski et al.
 415 (2006) with initial conditions and forcings taken from Böing et al. (2012). The relative
 416 humidity was held constant and equal to 80% up to an altitude of 6,000 m, and then
 417 decreased linearly to 15% at 17,500 m. The potential temperature was computed from
 418 a prescribed lapse rate following a simple function of altitude, while horizontal winds were
 419 initially set to 0 m s⁻¹ everywhere. Latent and sensible surface heat fluxes were held con-
 420 stant throughout the simulation and equal to 343 W m⁻² and 161 W m⁻² respectively,
 421 which corresponds to the diurnal averages of the time-dependent fluxes imposed in Grabowski
 422 et al. (2006). Horizontal winds were nudged back to their initial values with a time scale
 423 of 6 hr over the course of the simulation, but no other external forcing (including radi-
 424 ation and large-scale advection) was imposed.

425 The simulation was performed using the MISU-MIT Cloud and Aerosol model (MIMICA;
 426 Savre et al., 2014) as described in Savre and Craig (2023). The numerical domain ex-
 427 tends over 102.4 km in both horizontal directions, and the upper boundary is situated
 428 14,250 m above the surface. The horizontal grid spacing is equal to 100 m in both di-
 429 rections, while the vertical grid spacing is constant and equal to 25 m below 1500 m, but
 430 increases geometrically above to reach ~ 400 m in the topmost grid layer. Lateral bound-

431 aries are periodic, whereas the surface is considered as a free-slip boundary (no momen-
 432 tum fluxes).

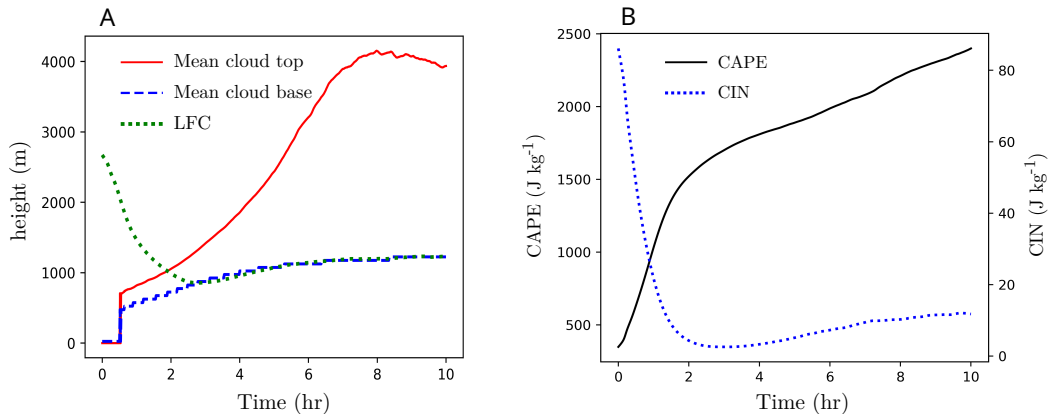


Figure 5. Shallow-to-deep transition in the idealized LBA case. (A) Time series of mean cloud top (red solid line), mean cloud base (blue dashed line), and LFC (green dotted line). (B) Time series of CAPE (black solid line) and CIN (blue dotted line).

433 The simulation was continued over a period of 10 hr, during which time-dependent
 434 variables were extracted every minute. The first clouds are observed 1 hr after the start
 435 of the simulation, whereas the onset of surface precipitation occurs 1.5 hr later. Over-
 436 all, the transition from shallow-to-deep convection happens progressively over the first
 437 7 hr of simulation. In Figure 5A, the mean cloud base and mean cloud top altitudes are
 438 shown. Here, the mean cloud base is defined as the level at which the cloud cover is max-
 439 imum, and the mean cloud top is defined as the first vertical layer from the top where
 440 the condensed water mixing ratio exceeds $10^{-3} \text{ g kg}^{-1}$. Clouds are identified at locations
 441 where the condensed water mixing ratio exceeds a threshold of $10^{-3} \text{ g kg}^{-1}$. In addition,
 442 the level of free convection (LFC) is also represented. As one may see, after around 3
 443 hr the mean cloud base altitude is almost identical to the LFC. The time evolution of
 444 CAPE and CIN is also represented in Figure 5B. CIN becomes very small after 2 hr, grad-
 445 ually increasing during the shallow-to-deep transition to about 10 J kg^{-1} . Here, we con-
 446 sider the shallow-to-deep convection transition to begin 2.5 hr after the start of the sim-
 447 ulation. During the transition, CAPE increases from about 1600 J kg^{-1} to about 2000
 448 J kg^{-1} .

449 The total cloud cover σ and cloud cover associated with precipitating convection
 450 σ_c that will be used to validate the predator-prey model are defined as follows. The to-
 451 tal cloud cover is computed as the ratio between the number of grid cells identified as
 452 cloudy at the mean cloud base altitude to the total number of grid cells at that level.
 453 The cloud cover of convective precipitating clouds is defined following the same proce-
 454 dure but 4 km above the surface. In Figure 6A, simulated total and precipitating cloud
 455 covers are shown together with a solution of the Lotka-Volterra model in which the cloud
 456 fraction at cloud base (total cloud population) is assumed to act as prey, and the cloud
 457 fraction at 4 km (precipitating cloud population) is assumed to act as predator. The Lotka-
 458 Volterra model is solved using the simple Euler method with 10^4 iterations (a conver-
 459 gence test with 10^3 iterations has been performed, showing no significant difference). Here,
 460 the Lotka-Volterra model is represented only to show the predator-prey characteristic
 461 of the system, and thus, no objective tuning of coefficients against the LES data has been
 462 performed: the coefficients were simply chosen to visually match the LES data. As can
 463 be seen from Figure 6A, even a very simple predator-prey system can model reasonably

464 well the rapid transition from shallow to deep continental convection, however, far from
 465 being a perfect model. As speculated above, σ_c can indeed act as a predator. We show
 466 in particular that the cloud cover decreases as the fraction of convective clouds at a higher
 467 level increases. Later, as the total cloud cover decreases, the number of clouds that pro-
 468 vide local preconditioning for the subsequent convection also decreases, and thus, the pop-
 469 ulation of predators (precipitating clouds) will decrease as they no longer have enough
 470 preys to feed on.

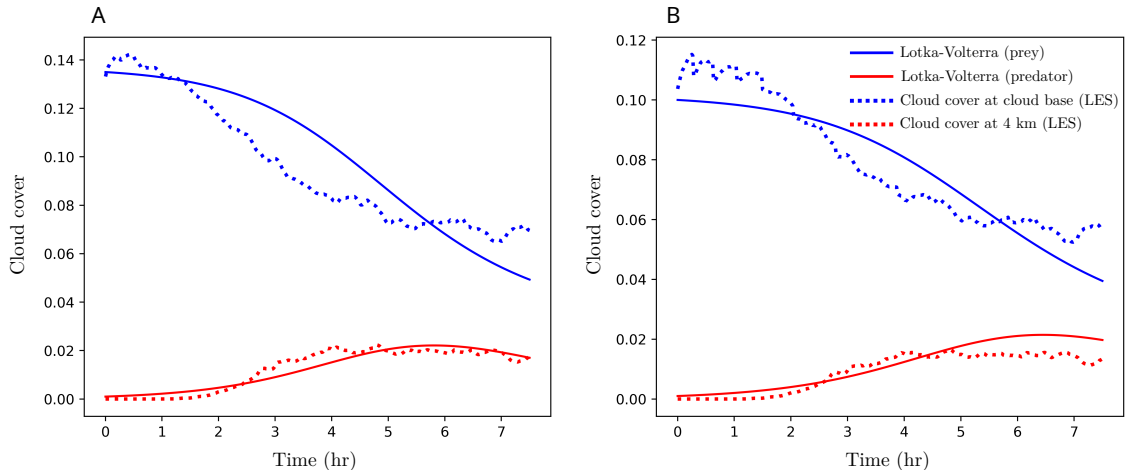


Figure 6. Lotka–Volterra model (solid lines) vs. LES data (dotted lines) for the LBA transi-
 tion case. (A) Cloud cover at the cloud base as prey (blue lines) and cloud cover at 4 km height
 as predators (red lines). (B) As in (A) but for cloudy updraft cover. For the Lotka–Volterra
 model, the following coefficients are considered: $a = 0$, $b = 3 \cdot 10^{-3} \text{ s}^{-1}$, $e = 3.5 \cdot 10^{-3} \text{ s}^{-1}$,
 $f = 2.5 \cdot 10^{-4} \text{ s}^{-1}$ (A); and $a = 0$, $b = 3 \cdot 10^{-3} \text{ s}^{-1}$, $e = 4 \cdot 10^{-3} \text{ s}^{-1}$, $f = 2 \cdot 10^{-4} \text{ s}^{-1}$ (B). The
 initial conditions are set to 0.135 for the cloud cover at the cloud base, 0.1 for the cloudy updraft
 cover at the cloud base, and 10^{-3} for the cloud cover and for the cloudy updraft at 4 km. Here,
 the initial time is set to 2.5 hr after the start of the simulation.

471 Because the cloudy updrafts are regarded as the fundamental agents of vertical con-
 472 vective transport in the mass–flux parameterization, we also analyze here the predator–
 473 prey characteristics of cloud cover with clouds identified based on an additional updraft
 474 criterion. Here, a threshold of 0.1 m s^{-1} is used to identify the cloudy updrafts. The predator–
 475 prey characteristics of cloud cover based on this additional updraft criterion (cloudy up-
 476 draft cover) are presented in Figure 6B. As speculated above, the cloudy updrafts cover
 477 also follows predator–prey characteristics, like the total cloud population. The predator–
 478 prey characteristics can be seen from the fact that the cloudy updraft cover at cloud base
 479 decreases as the cloudy updraft cover at 4 km increases in the first part of the transi-
 480 tion. This is followed by a decrease in the cloudy updraft cover at 4 km as the number
 481 of prey becomes too small. Note that Yano and Plant (2012b) argue that during the shallow–
 482 to–deep transition, as CAPE increases, the cloudy updraft cover at cloud base also in-
 483 creases, but without giving any physical argument to support this assertion. However,
 484 it is quite clear from Figure 6B that for the rapid shallow–to–deep transition discussed
 485 here, the cloud cover at the cloud base exhibits a decrease during the transition, even
 486 though CAPE does increase.

487 As a first order approximation, we can consider that the surface precipitation rate
 488 P is directly proportional to σ_c . Similar to Koren and Feingold (2011), we may there-

489 fore replace σ_c with P in equations 7–8, thus considering that the surface precipitation rate acts as a predator that preys on the total cloud fraction. We then expect to see a
 490 time series for the cloud–precipitation system resembling that displayed on Figure 4A,
 491 and a solution for the cloud cover and precipitation rate similar to the one showed on
 492 Figure 4B.
 493

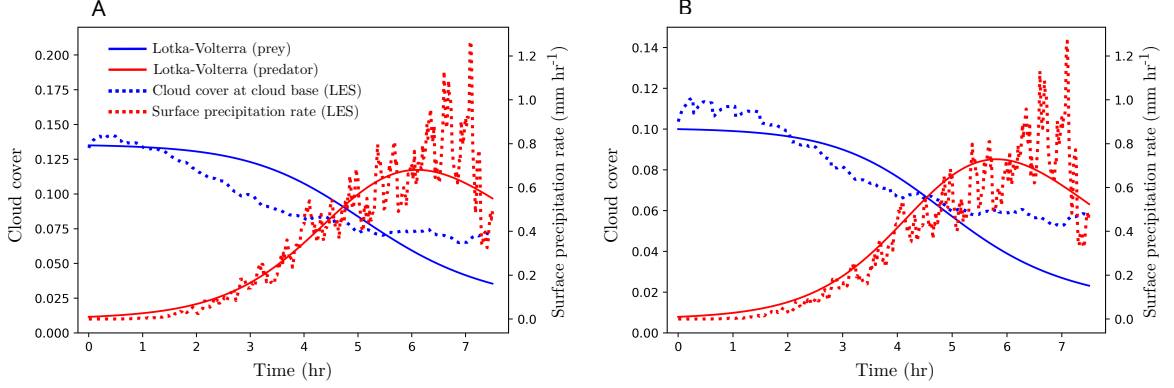


Figure 7. As in Figure 6 but the with surface precipitation rate acting as predators. For the Lotka–Volterra model, the following coefficients are considered: $a = 0$, $b = 1.5 \cdot 10^{-4} \text{ hr mm}^{-1} \text{ s}^{-1}$, $e = 3.5 \cdot 10^{-3} \text{ s}^{-1}$, $f = 2 \cdot 10^{-4} \text{ s}^{-1}$ (A); and $a = 0$, $b = 1.5 \cdot 10^{-4} \text{ hr mm}^{-1} \text{ s}^{-1}$, $e = 5 \cdot 10^{-3} \text{ s}^{-1}$, $f = 2.1 \cdot 10^{-4} \text{ s}^{-1}$ (B). The initial surface precipitation rate is set to $10^{-3} \text{ mm hr}^{-1}$.

494 In Figure 7, the time series of cloud cover at cloud base and surface precipitation
 495 rate are presented, together with a solution of the Lotka–Volterra model in which the
 496 cloud fraction at cloud base is assumed to act as prey, and the surface precipitation rate
 497 is assumed to act as predator. The surface precipitation rate displayed in Figure 7 rep-
 498 represents the domain–averaged surface precipitation rate. Indeed, the cloud–precipitations
 499 system exhibits predator–prey characteristics during the rapid shallow–to–deep transi-
 500 tion, as speculated above. Although not perfect, the Lotka–Volterra model does seem
 501 to represent reasonably well the interaction between clouds and precipitation.

502 3.2 Extension to a three species model

503 An extension to a three species model can be made by considering that the convective
 504 precipitating clouds can be further classified as congestus and cumulonimbus clouds. Here,
 505 we consider that the congestus clouds are those clouds with a top between 4 km and 8
 506 km, whereas the cumulonimbus clouds have a top above 8 km. Therefore, we consider
 507 that the cloud cover at the cloud base (total cloud population) acts as prey for the cloud
 508 cover at 4 km σ_c (convective precipitating cloud population), which also represents the
 509 prey for the cloud cover at 8 km σ_{cb} (cumulonimbus cloud cover). Hence, we have the
 510 following predator–prey system:

$$\frac{d\sigma}{dt} = \beta_1\sigma - \beta_2\sigma\sigma_c, \quad (9)$$

$$\frac{d\sigma_c}{dt} = \beta_3\sigma\sigma_c - \beta_4\sigma_c\sigma_{cb} - \beta_5\sigma_c, \quad (10)$$

$$\frac{d\sigma_{cb}}{dt} = \beta_6\sigma_c\sigma_{cb} - \beta_7\sigma_{cb}, \quad (11)$$

511 where β_1 – β_7 are system coefficients. A solution to this system is presented in Figure 8,
 512 together with time series of cloud cover at the cloud base (Figure 8A), 4 km (Figure 8B),
 513 and 8 km (Figure 8C), from the LBA transition case described above. Comparing the
 514 LES data for the cloud cover at these three levels with the solution of the Lotka–Volterra
 515 model, the system seems to exhibit predator–prey characteristics with three species.

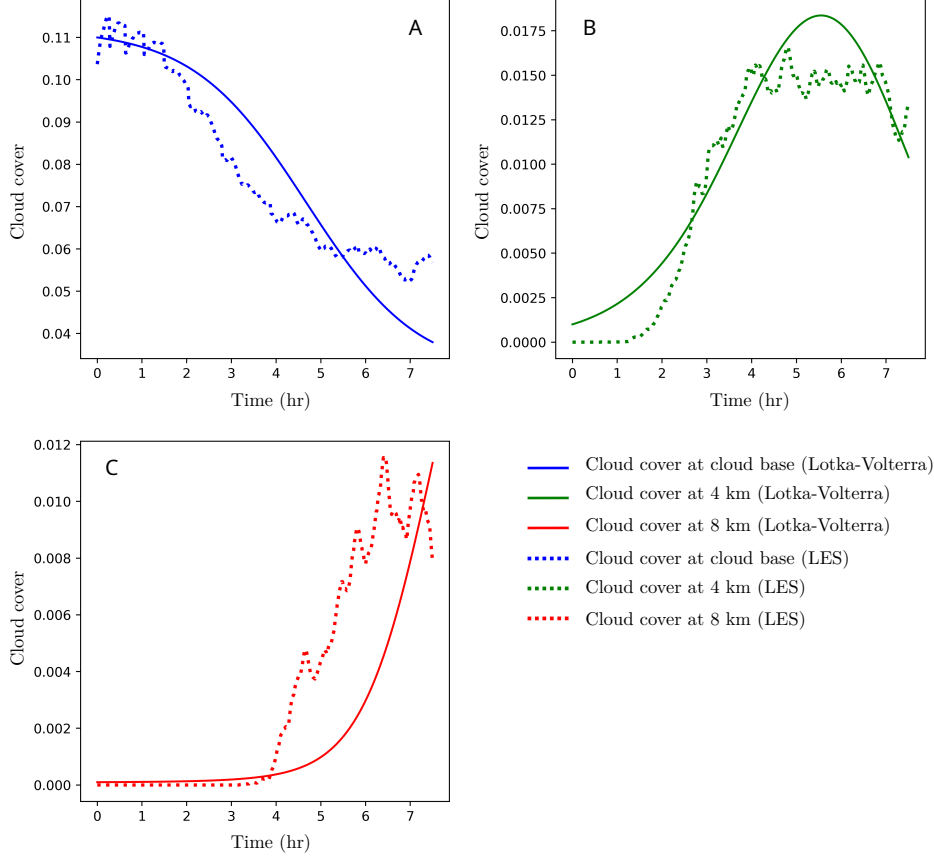


Figure 8. Three species Lotka–Volterra model (solid lines) vs. LES data (dotted lines) for the LBA transition case. (A) Cloudy updraft cover at the cloud base as prey (blue lines); (B) Cloudy cover at the 4 km height representing the convective fractional area of congestus and cumulonimbus clouds; (C) Cloudy cover at the 8 km height representing the convective fractional area of cumulonimbus clouds. For the Lotka–Volterra model, the following coefficients are considered: $\beta_1 = 0$, $\beta_2 = 3.8 \cdot 10^{-3} \text{ s}^{-1}$, $\beta_3 = 3.8 \cdot 10^{-3} \text{ s}^{-1}$, $\beta_4 = 10^{-2} \text{ s}^{-1}$, $\beta_5 = 2 \cdot 10^{-4} \text{ s}^{-1}$, $\beta_6 = 1.7 \cdot 10^{-2} \text{ s}^{-1}$, $\beta_7 = 10^{-6} \text{ s}^{-1}$. The initial conditions are set to 0.11, 10^{-3} , and 10^{-4} for the cloudy updraft cover at the cloud base, at 4 km, and 8 km, respectively.

516 Further extension to n_z species, where n_z represents the number of vertical levels
 517 used by the parent numerical model, follows immediately. For the updraft fractional area
 518 σ_k at the vertical level k , we now have:

$$\frac{d\sigma_k}{dt} = a_{k,k-1}\sigma_k\sigma_{k-1} - a_{k,k+1}\sigma_k\sigma_{k+1} + r_k\sigma_k, \quad (12)$$

519 where $a_{k,k-1}$, $a_{k,k+1}$, and r_k are system coefficients. The number of species represents
 520 the number of vertical levels of the parent numerical model between LFC and the equi-
 521 librium level.

522 3.3 LBA Transition Case with Suppressed Cold Pools

523 As discussed in Section 2, in our conceptual model, the predator–prey characteristics for
 524 the shallow–to–deep transition is due to the local moisture preconditioning, with the cold
 525 pool feedback only acting as a reinforcement. Thus, we argue that predator–prey behav-
 526 ior is expected even in the absence of the cold pools. To test this aspect, an additional
 527 simulation with suppressed cold pools is performed. The strategy proposed by Böing et
 528 al. (2012) was adopted here whereby potential temperature and water vapor mixing ra-
 529 tio tendencies below cloud base are nudged to their horizontally averaged values with
 530 a time scale of 10 min.

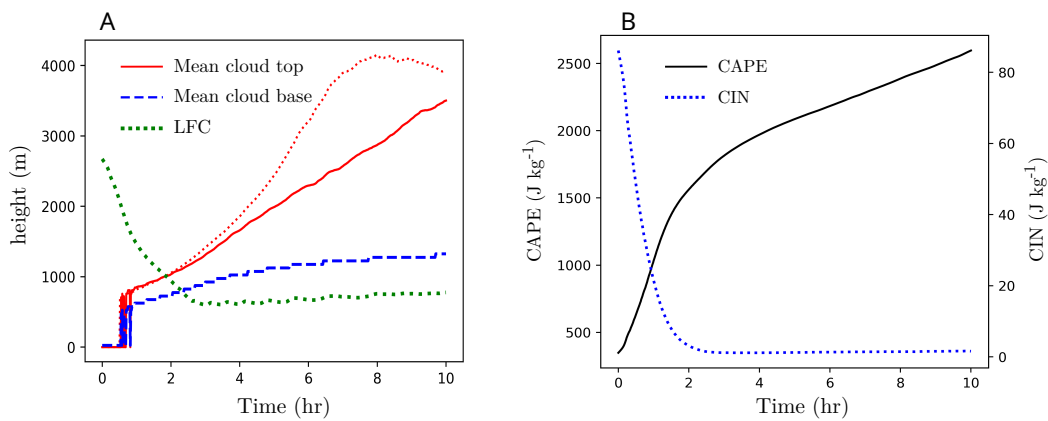


Figure 9. As in Figure 5, but for the case with suppressed cold pools. The mean cloud top for the case with active cold pools is also displayed here with red dotted line.

531 In Figure 9A, the mean cloud top, mean cloud base, and LFC are presented. The
 532 mean cloud top for the case with active cold pools is also presented here to better ap-
 533 preciate the cold pool feedback in the shallow–to–deep transition. As expected, the tran-
 534 sition is slower for the case with suppressed cold pools, although there is not a large dif-
 535 ference between the mean cloud top for the two cases in the first part of the transition,
 536 during which we argue that the role of local preconditioning is the main mechanism re-
 537 sponsible for the transition. As another interesting aspect, in this case, the LFC is lower
 538 than the mean cloud base during the shallow–to–deep transition. As in the case with ac-
 539 tive cold pools, we consider that the transition starts at 2.5 hr after the start of the simu-
 540 lation, but the cloud top does not reach a maximum even after 10 hr, at the end of the
 541 simulation. The time series for CAPE and CIN is represented in Figure 9B. Although
 542 CAPE increases in a similar fashion to the case with active cold pools, CIN reaches a
 543 minimum after around 2.5 hr, remaining rather constant during the transition, at a value
 544 of about 1.5 J kg^{-1} . In addition, LFC is also much lower in the case with suppressed cold
 545 pools (around 0.7 km) than in the case with active cold pools (around 1 km).

546 In Figure 10, the cloudy updrafts covers at cloud base, 4 km, and 8 km, are repre-
 547 sented for the case with suppressed cold pools, together with a solution of the three species
 548 Lotka–Volterra model. As speculated, even without cold pools, the system seems to ex-
 549 hibit predator–prey characteristics. In order to appreciate the role of the cold pool feed-
 550 back in the transition, we also represent the cloudy updrafts covers for the case with ac-

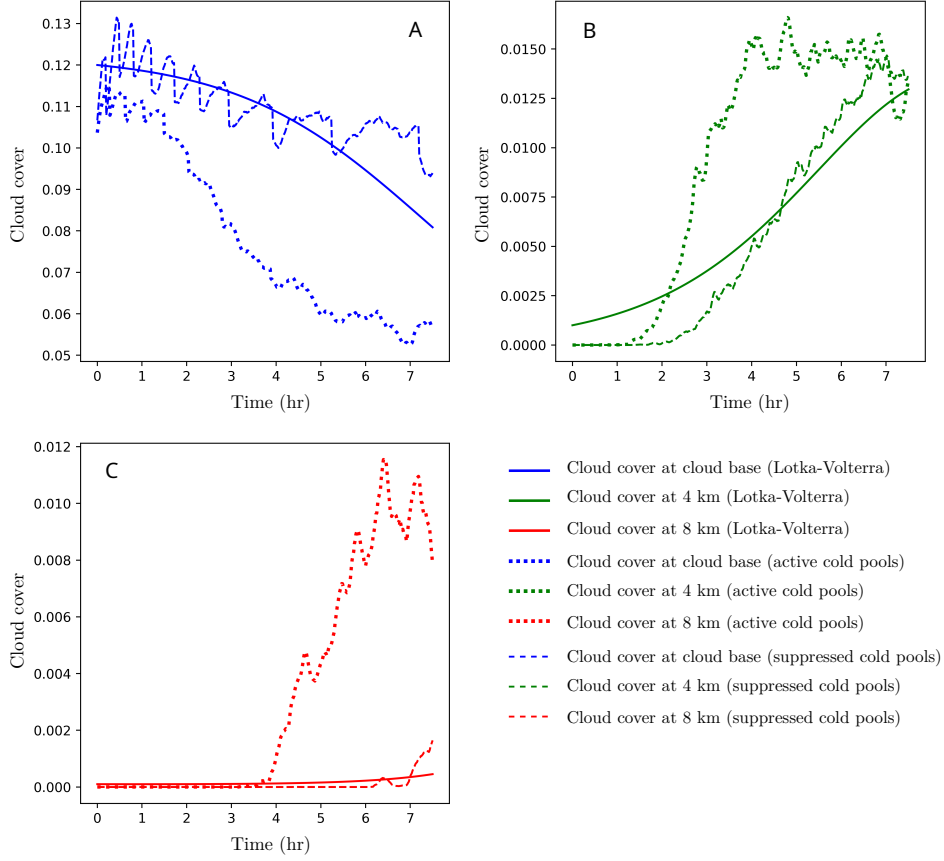


Figure 10. As in Figure 8, but for the case with suppressed cold pools. The cloudy updraft covers for the case with active cold pools are also displayed here with dotted lines, while the cloudy updraft covers for the case with suppressed cold pools are represented with dashed lines. For the Lotka–Volterra model, the following coefficients are considered: $\beta_1 = 0$, $\beta_2 = 2.5 \cdot 10^{-3} \text{ s}^{-1}$, $\beta_3 = 2.5 \cdot 10^{-3} \text{ s}^{-1}$, $\beta_4 = 10^{-2} \text{ s}^{-1}$, $\beta_5 = 1.7 \cdot 10^{-4} \text{ s}^{-1}$, $\beta_6 = 1.3 \cdot 10^{-2} \text{ s}^{-1}$, $\beta_7 = 2 \cdot 10^{-5} \text{ s}^{-1}$. The initial conditions are set to 0.12, 10^{-3} , and 10^{-4} for the cloudy updraft cover at the cloud base, at 4 km, and 8 km, respectively.

551 tive cold pools. As we expected from the conceptual model, without cold pool feedback
 552 the predators are not that efficient in preying on the total cloud population, and thus
 553 the cloud cover at the cloud base does not decrease as fast as the cloud cover for the case
 554 with active cold pools, while the populations of convective precipitating clouds and cumulonimbus clouds are not able to grow as fast and as much as for the case with active
 555 cold pools. Moreover, with suppressed cold pools, a larger number of updrafts are able
 556 to reach the condensation level as CIN is lower and there is no organization of the up-
 557 draft field in the boundary layer.
 558

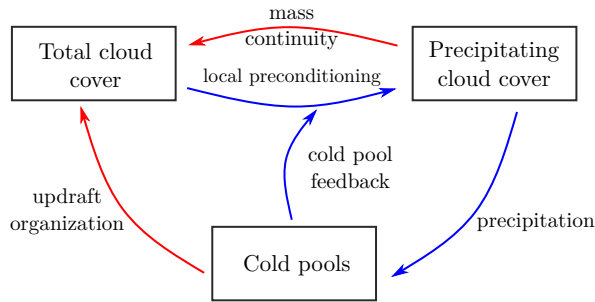


Figure 11. Schematics of feedback between the clouds and cold pools. The blue arrow denotes a positive causality, while the red one denotes a negative causality.

559 Although there is a significant difference in the number of cumulonimbus clouds
 560 between the two simulations, it is clear that the deepening of cumulus convection is possible even without cold pools feedback. This aspect, together with the predator–prey characteristics of the case with suppressed cold pools, indicates that the local preconditioning plays a major role in the shallow–to–deep transition, as also argued by Vraciu et al. (2023), and we believe that much more attention should be given to the local moisture preconditioning, and to the interplay between the local preconditioning and cold pools feedback during the transition from shallow to precipitating convection. We schematically present the feedback loops between the clouds and cold pools in our conceptual model on Figure 11. A negative feedback loop between the total cloud cover and precipitating cloud cover is possible without the presence of the cold pools, due to local preconditioning and mass continuity, implying a predator–prey–type of interaction between the two. As the precipitating clouds start to precipitate in their decaying state, cold pools are formed in the boundary layer, which have a positive effect on the population of precipitating clouds, but also a direct negative effect on the total cloud cover due to the organization of updrafts in the boundary layer, as discussed in Section 2.2. As the cold pools have a positive feedback on the population of precipitating clouds, due to mass continuity, the cold pools also have an indirect negative effect on the total cloud cover, as also schematically illustrated in Figure 3. Here, the arrow of the cold pools feedback points towards local preconditioning, as in our conceptual model the cold pools, through the organization of updrafts, increase the probability of updrafts feeding into preexisting clouds, and thus, leading to a larger degree of local preconditioning, as also discussed in Section 2.2. Overall, the cold pools amplify the feedback loop between the total cloud cover (prey) and the precipitating cloud cover (predator), which can be seen as making the predators more efficient in catching the prey. In this sense perhaps, the cold pools may be seen as mountains forcing the preys and predators to live into narrow valleys (the gust fronts), thus facilitating the interactions between them.
 585

586

3.4 Complete Diurnal Cycle

587

588

589

590

591

592

593

594

595

To see if within a complete diurnal cycle the cloud–precipitation system exhibits predator–prey characteristics, we consider here the idealized case reported in Jensen et al. (2022) that is openly available at Haerter (2021). The reader is referred to Jensen et al. (2022) for case description and methodological details. In a complete diurnal cycle, we can no longer ignore the contribution of the surface heat flux on σ . Thus, we can no longer assume that the Lotka–Volterra system, in which there is no external forcing, can describe the interaction between the cloud cover and precipitation rate. However, during the transition from shallow to precipitation convection, we still expect to see a predator–prey type of interaction.

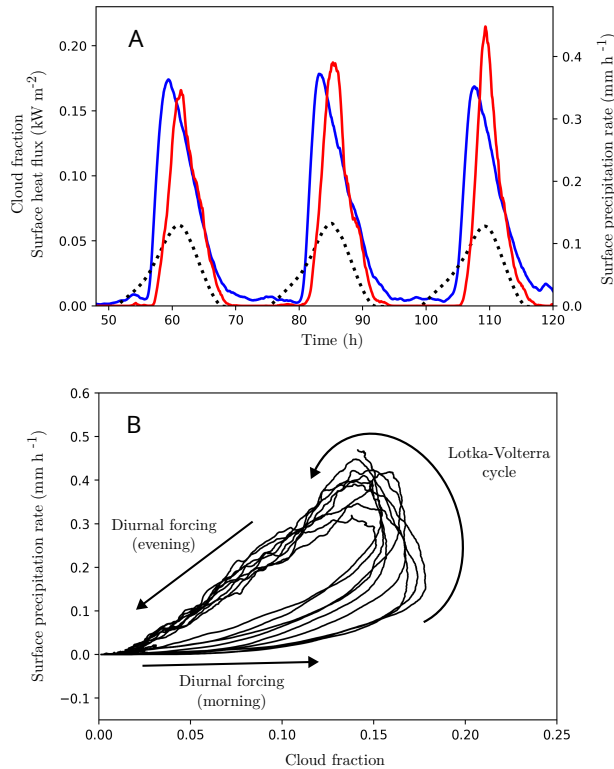


Figure 12. Large-eddy simulation of the cloud–precipitation system in a complete diurnal cycle from Jensen et al. (2022). (A) Time series for cloud fraction (blue solid line) and surface precipitation rate (red solid line) for three complete diurnal cycles. The surface heat flux is also represented for reference (dotted black line). (B) Limit–cycle of the cloud–precipitation system for the complete simulation (10 days), except the first two days, which are considered spin–up time.

596

597

598

599

600

601

602

603

In Figure 12, the LES data for cloud cover and surface precipitation from Jensen et al. (2022) are represented. In the morning, during the onset of the shallow convection, the cloud population increases as more and more updrafts are able to overcome the transition layer and reach the condensation level, and thus, the evolution of the cloud fraction is dominated by the diurnal forcing associated with the surface fluxes. As CIN approaches zero, the transition from shallow to precipitation convection starts, and indeed, during this short period, we see predator–prey characteristics in the cloud–precipitation system (Figure 12A), which correspond to the upper–right portion of the limit–cycle (Fig-

604 ure 12B). Thus, during the transition, in agreement with our conceptual model, the cloud
 605 fraction decreases as the precipitation rate increases, which in turn leads to a reduction
 606 in the precipitation rate. During the evening, as the surface heat flux is unable to pro-
 607 vide enough energy into the system, and CIN is slowly restored. Thus, the cloud frac-
 608 tion decreases as the clouds that decay are no longer replaced by new active clouds, and
 609 the cloud population is again controlled by the diurnal forcing.

610 Although Figure 12 suggests that even within a complete diurnal cycle the system
 611 exhibits predator–prey characteristics, our simple Lotka–Volterra model is only able to
 612 represent the transition phase happening during the day. The model is indeed unable
 613 to represent the simultaneous decay of both shallow and deep cumuli at night when the
 614 reduced surface fluxes cannot sustain convection. A predator–prey model that takes into
 615 consideration this diurnal forcing might however be designed and adjusted to reproduce
 616 the complete diurnal cycle of cloud and precipitation. In this context, surface fluxes might
 617 be modeled as an external food supply for the preys in a biological system.

618 4 Discussion and Conclusions

619 In this study, we consider that the cumulus clouds are formed due to the upward trans-
 620 port of water vapor from the boundary layer by multiple convective elements, as sug-
 621 gested by empirical evidence. As the clouds themselves precondition their local surround-
 622 ings for the subsequent convective updrafts, it is considered that the convective precip-
 623 itating clouds act as predators, eating from the total cloud fraction that sustains their
 624 growth. As the clouds become deeper, the total cloud fraction decreases, and thus, the
 625 total cloud population can be seen as the prey population in a predator–prey system.
 626 It is also argued that the cold pool feedback acts as a reinforcement mechanism, lead-
 627 ing to more clustered convection. The conceptual picture for the shallow-to-deep con-
 628 vection reminds us of the transition from unorganized to aggregated convection, but at
 629 a smaller scale. Therefore, we argue that the very complex cloud dynamics in the rapid
 630 shallow–to–deep transition of atmospheric convection can be described by the very sim-
 631 ple Lotka–Volterra predator–prey system if it is assumed that the change in the large-
 632 scale state is slow enough during the transition. We tested a simple predator–prey model
 633 against idealized high–resolution LES data, showing good agreement between them. To
 634 isolate the role of local moisture preconditioning from that of cold pool feedback, we also
 635 consider a twin LES simulation with suppressed cold pools. In agreement with our con-
 636 ceptual model, the transition displays predator–prey characteristics even without cold
 637 pools, which might be an indication that the local preconditioning plays an important
 638 role in the shallow–to–deep transition. Finally, we discuss the complete diurnal cycle of
 639 deep convection, showing that the cloud population also exhibits a predator–prey–type
 640 of behavior in this situation. We consider that future research is required to study in depth
 641 every causality implied by our study, which might help us better understand the com-
 642 plex process of storm formation and convective organization.

643 In a diurnal cycle of deep continental convection, the predator–prey model assumes
 644 a gradual transition to deep convection instead of assuming an instantaneous deep con-
 645 vection triggering. The majority of current mass–flux schemes for deep convection con-
 646 sider a constant fractional area occupied by the convection, either explicitly or implic-
 647 itly. However, in a rapid transition from shallow to precipitating deep convection, the
 648 environmental state only exhibits a small change, and the convective mass–flux is pri-
 649 marily controlled by convective fractional area and not by the vertical velocity. There-
 650 fore, our predator–prey model may be implemented for such a case by replacing the mass-
 651 flux predicted by the deep convection scheme M'_c with an adjusted mass–flux $M_{c,adj}$, as
 652 follows:

$$M_{c,adj} = \frac{\sigma_c}{\sigma'_c} M'_c, \quad (13)$$

653 where σ_c is the fraction of convective precipitating clouds from the predator–prey model,
 654 and σ'_c is the constant fractional area assumed by the deep convection schemes. If the
 655 scheme does not assume a fractional area in an explicit way, then a constant value for
 656 σ'_c must be prescribed. Therefore, a predator–prey model may be implemented in a weather
 657 prediction or climate numerical model, obtaining a cumulus parameterization scheme with
 658 convective memory, that is based on a more realistic conceptual picture than the tradi-
 659 tional mass–flux formulation, that goes beyond the one-cloud equals one-updraft frame-
 660 work. It should be noted, however, that this implementation cannot be made if the deep
 661 convective scheme already has a parameterization for the cold pool feedback (e.g., Rio
 662 et al., 2009; Suselj et al., 2019), as this would lead to a ‘double counting’ of the cold pools
 663 effect. Such an implementation, however, can only be made during the shallow–to–deep
 664 transition, as it is considered that the environment does not change substantially. There-
 665 fore, the predator–prey model must only be turned on when the conditions for deep con-
 666 vection onset are met and turned off after deep convection fully develops. Moreover, as
 667 shown in Section 3.2, the predator–prey system can be further generalized, to predict
 668 the convective fractional area at every vertical level of the numerical model. Future re-
 669 search is required to find the most appropriate predator–prey system for the shallow–
 670 to–deep transition and to tune the various coefficients introduced by the model.

671 As another very important contribution of the present conceptual model, a unified
 672 convection–cloud picture is described in which both clouds and convective elements in-
 673 teract with each other. Thus, the present predator–prey model also provides a param-
 674 eterization for the total cumulus fraction, a problem notorious for the climate projec-
 675 tions (e.g., Vogel et al., 2022). In addition, a complete unified parameterization might
 676 be built based on the principles introduced here by considering the prognostic Equation
 677 5 for the cloud fraction, and a bulk plume model that considers the local precondition-
 678 ing, as proposed for example by Vraciu et al. (2023). In the Vraciu et al. (2023) bulk plume
 679 model, a closure for the fraction of cloudy air entrained by the updrafts is required. How-
 680 ever, based on the predator–prey model described here, it might be considered that the
 681 predators are those updrafts that only entrain moist cloudy air, obtaining thus the frac-
 682 tion as the ratio between the predators and the prey. Furthermore, note that by con-
 683 sidering Equation 5, the boundary layer control of deep convection is implicit, in con-
 684 trast with the traditional mass–flux formulation in which a boundary layer control, al-
 685 though considered by many modern parameterizations, might be in fact inconsistent with
 686 the steady–state plume model of the mass–flux formulation (please refer to Yano et al.
 687 (2013) for a detailed discussion of this issue). Such a development is not presented here
 688 but left for future work.

689 Open Research

690 The LES data presented in Sections 3.1 and 3.2 of this work are openly available
 691 at Savre (2023a), while the data presented in Section 3.3 are available at Savre (2023b).
 692 The data presented in Figure 12 are openly available at Haerter (2021).

693 Acknowledgments

694 The authors thank Robert Plant for insightful comments and feedback. CVV ac-
 695 knowledges financial support from the Romanian Ministry of Research, Innovation, and
 696 Digitization through Project PN 23 21 01 01 and from the Romanian Ministry of Ed-
 697 ucation consisting in a doctoral scholarship received through the Doctoral School of Physics
 698 of the University of Bucharest.

699 References

700 Albright, A. L., Bony, S., Stevens, B., & Vogel, R. (2022). Observed subcloud-layer

- 701 moisture and heat budgets in the trades. *Journal of the Atmospheric Sciences*,
702 79(9), 2363–2385.
- 703 Albright, A. L., Stevens, B., Bony, S., & Vogel, R. (2023). A new conceptual picture
704 of the trade wind transition layer. *Journal of the Atmospheric Sciences*, 80(6),
705 1547–1563.
- 706 Arakawa, A. (2004). The cumulus parameterization problem: Past, present, and fu-
707 ture. *Journal of Climate*, 17(13), 2493–2525.
- 708 Arakawa, A., & Schubert, W. H. (1974). Interaction of a cumulus cloud ensemble
709 with the large-scale environment, Part I. *Journal of the Atmospheric Sciences*,
710 31(3), 674–701.
- 711 Bechtold, P., Bazile, E., Guichard, F., Mascart, P., & Richard, E. (2001). A mass-
712 flux convection scheme for regional and global models. *Quarterly Journal of*
713 *the Royal Meteorological Society*, 127(573), 869–886.
- 714 Bechtold, P., Chaboureaud, J.-P., Beljaars, A., Betts, A., Köhler, M., Miller, M., &
715 Redelsperger, J.-L. (2004). The simulation of the diurnal cycle of convective
716 precipitation over land in a global model. *Quarterly Journal of the Royal*
717 *Meteorological Society*, 130(604), 3119–3137.
- 718 Bechtold, P., Semane, N., Lopez, P., Chaboureaud, J.-P., Beljaars, A., & Bormann, N.
719 (2014). Representing equilibrium and nonequilibrium convection in large-scale
720 models. *Journal of the Atmospheric Sciences*, 71(2), 734–753.
- 721 Betts, A. K. (1976). Modeling subcloud layer structure and interaction with a shal-
722 low cumulus layer. *Journal of the Atmospheric Sciences*, 33(12), 2363–2382.
- 723 Böing, S. J., Jonker, H. J. J., Siebesma, A. P., & Grabowski, W. W. (2012).
724 Influence of the subcloud layer on the development of a deep convective
725 ensemble. *Journal of the Atmospheric Sciences*, 69, 2682–2698. doi:
726 10.1175/JAS-D-11-0317.1
- 727 Bretherton, C. S., McCaa, J. R., & Grenier, H. (2004). A new parameterization for
728 shallow cumulus convection and its application to marine subtropical cloud-
729 topped boundary layers. Part I: Description and 1D results. *Monthly Weather*
730 *Review*, 132(4), 864–882.
- 731 Champouillon, A., Rio, C., & Couvreux, F. (2023). Simulating the transition from
732 shallow to deep convection across scales: The role of congestus clouds. *Journal*
733 *of the Atmospheric Sciences*, 80(12), 2989–3005.
- 734 Christopoulos, C., & Schneider, T. (2021). Assessing biases and climate implications
735 of the diurnal precipitation cycle in climate models. *Geophysical Research Let-*
736 *ters*, 48(13), e2021GL093017.
- 737 Colin, M., Sherwood, S., Geoffroy, O., Bony, S., & Fuchs, D. (2019). Identifying the
738 sources of convective memory in cloud-resolving simulations. *Journal of the At-*
739 *mospheric Sciences*, 76(3), 947–962.
- 740 Colin, M., & Sherwood, S. C. (2021). Atmospheric convection as an unstable
741 predator–prey process with memory. *Journal of the Atmospheric Sciences*,
742 78(11), 3781–3797.
- 743 Couvreux, F., Roehrig, R., Rio, C., Lefebvre, M.-P., Komori, T., Derbyshire, S., ...
744 others (2015). Representation of daytime moist convection over the semi-
745 arid tropics by parametrizations used in climate and meteorological models.
746 *Quarterly Journal of the Royal Meteorological Society*, 141(691), 2220–2236.
- 747 Daleu, C. L., Plant, R., Woolnough, S., Stirling, A., & Harvey, N. (2020). Memory
748 properties in cloud-resolving simulations of the diurnal cycle of deep convec-
749 tion. *Journal of Advances in Modeling Earth Systems*, 12(8), e2019MS001897.
- 750 Damiani, R., Vali, G., & Haimov, S. (2006). The structure of thermals in cumu-
751 lus from airborne dual-Doppler radar observations. *Journal of the Atmospheric*
752 *Sciences*, 63(5), 1432–1450.
- 753 Davies, L., Plant, R., & Derbyshire, S. (2013). Departures from convective equi-
754 librium with a rapidly varying surface forcing. *Quarterly Journal of the Royal*
755 *Meteorological Society*, 139(676), 1731–1746.

- 756 Donner, L. J. (1993). A cumulus parameterization including mass fluxes, vertical
757 momentum dynamics, and mesoscale effects. *Journal of the Atmospheric Sci-*
758 *ences*, 50(6), 889–906.
- 759 Donner, L. J., & Phillips, V. T. (2003). Boundary layer control on convective avail-
760 able potential energy: Implications for cumulus parameterization. *Journal of*
761 *Geophysical Research: Atmospheres*, 108(D22), 4701.
- 762 Emanuel, K. A. (1991). A scheme for representing cumulus convection in large-scale
763 models. *Journal of the Atmospheric Sciences*, 48(21), 2313–2329.
- 764 Emanuel, K. A. (1993). A cumulus representation based on the episodic mixing
765 model: the importance of mixing and microphysics in predicting humidity. In
766 *The representation of cumulus convection in numerical models* (pp. 185–192).
767 Springer.
- 768 Grabowski, W. (2023). Daytime convective development over land: The role of sur-
769 face forcing. *Quarterly Journal of the Royal Meteorological Society*, 149(756),
770 2800–2819.
- 771 Grabowski, W., Bechtold, P., Cheng, A., Forbes, R., et al. (2006). Daytime con-
772 vective development over land: A model intercomparison based on LBA ob-
773 servations. *Quarterly Journal of the Royal Meteorological Society*, 132(615),
774 317–344.
- 775 Haerter, J. O. (2021). 1D (time) and 2D (time and vertical coordinate) data for the
776 cases DIU-500m, RCE-500m and DIU2RCE-500m [Data set]. *Zenodo*. doi:
777 <https://doi.org/10.5281/zenodo.4898182>
- 778 Harrington, E. L. (1958). Observations on the appearance and growth of tropical cu-
779 muli. *Journal of the Atmospheric Sciences*, 15(2), 127–130.
- 780 Harvey, N. J., Daleu, C. L., Stratton, R. A., Plant, R. S., Woolnough, S. J., & Stir-
781 ling, A. J. (2022). The impact of surface heterogeneity on the diurnal cycle
782 of deep convection. *Quarterly Journal of the Royal Meteorological Society*,
783 148(749), 3509–3527.
- 784 Hernandez-Deckers, D., & Sherwood, S. C. (2016). A numerical investigation of cu-
785 mulus thermals. *Journal of the Atmospheric Sciences*, 73(10), 4117–4136.
- 786 Heus, T., Jonker, H. J. J., Van den Akker, H. E., Griffith, E. J., Koutek, M., & Post,
787 F. H. (2009). A statistical approach to the life cycle analysis of cumulus clouds
788 selected in a virtual reality environment. *Journal of Geophysical Research:*
789 *Atmospheres*, 114(D6).
- 790 Hohenegger, C., & Bretherton, C. S. (2011). Simulating deep convection with a shal-
791 low convection scheme. *Atmospheric Chemistry and Physics*, 11(20), 10389–
792 10406.
- 793 Hohenegger, C., & Stevens, B. (2013). Preconditioning deep convection with cumu-
794 lus congestus. *Journal of the Atmospheric Sciences*, 70(2), 448–464.
- 795 Holloway, C. E., & Neelin, J. D. (2009). Moisture vertical structure, column wa-
796 ter vapor, and tropical deep convection. *Journal of the Atmospheric Sciences*,
797 66(6), 1665–1683.
- 798 Hwong, Y.-L., Colin, M., Aglas-Leitner, P., Muller, C. J., & Sherwood, S. C. (2023).
799 Assessing memory in convection schemes using idealized tests. *Journal of Ad-*
800 *vances in Modeling Earth Systems*, 15(12), e2023MS003726.
- 801 Jensen, G. G., Fiévet, R., & Haerter, J. O. (2022). The diurnal path to persistent
802 convective self-aggregation. *Journal of Advances in Modeling Earth Systems*,
803 14(5), e2021MS002923.
- 804 Jones, T. R., & Randall, D. A. (2011). Quantifying the limits of convective parame-
805 terizations. *Journal of Geophysical Research: Atmospheres*, 116(D8).
- 806 Kain, J. S., & Fritsch, J. M. (1993). Convective parameterization for mesoscale mod-
807 els: The Kain-Fritsch scheme. In *The representation of cumulus convection in*
808 *numerical models* (pp. 165–170). Springer.
- 809 Khairoutdinov, M., & Randall, D. (2006). High-resolution simulation of shallow-
810 to-deep convection transition over land. *Journal of the Atmospheric Sciences*,

- 811 63(12), 3421–3436.
- 812 Kjoenbongarit. (2013). *Forming cumulonimbus (timelapse)*. [https://www.youtube](https://www.youtube.com/watch?v=232LFz-aiz4)
813 [.com/watch?v=232LFz-aiz4](https://www.youtube.com/watch?v=232LFz-aiz4). YouTube. (Accessed: 21.07.2023)
- 814 Koenig, L. R. (1963). The glaciating behavior of small cumulonimbus clouds. *Journal of Atmospheric Sciences*, 20(1), 29–47.
- 815
- 816 Koren, I., & Feingold, G. (2011). Aerosol–cloud–precipitation system as a predator–prey problem. *Proceedings of the National Academy of Sciences of the United States of America*, 108(30), 12227–12232.
- 817
- 818
- 819 Kurowski, M. J., Suselj, K., Grabowski, W. W., & Teixeira, J. (2018). Shallow-to-deep transition of continental moist convection: Cold pools, surface fluxes, and mesoscale organization. *Journal of the Atmospheric Sciences*, 75(12), 4071–4090.
- 820
- 821
- 822
- 823 Malkus, J. S., & Scorer, R. S. (1955). The erosion of cumulus towers. *Journal of the Atmospheric Sciences*, 12, 43–57.
- 824
- 825 Markowski, P., & Richardson, Y. (2011). *Mesoscale meteorology in midlatitudes*. John Wiley & Sons.
- 826
- 827 Meyer, B., & Haerter, J. O. (2020). Mechanical forcing of convection by cold pools: Collisions and energy scaling. *Journal of Advances in Modeling Earth Systems*, 12(11), e2020MS002281.
- 828
- 829
- 830 Moorthi, S., & Suarez, M. J. (1992). Relaxed arakawa-schubert. a parameterization of moist convection for general circulation models. *Monthly Weather Review*, 120(6), 978–1002.
- 831
- 832
- 833 Morrison, H. (2017). An analytic description of the structure and evolution of growing deep cumulus updrafts. *Journal of the Atmospheric Sciences*, 74(3), 809–834.
- 834
- 835
- 836 Morrison, H., Peters, J. M., Chandrakar, K. K., & Sherwood, S. C. (2022). Influences of environmental relative humidity and horizontal scale of subcloud ascent on deep convective initiation. *Journal of the Atmospheric Sciences*, 79(2), 337–359.
- 837
- 838
- 839
- 840 Morrison, H., Peters, J. M., Varble, A. C., Hannah, W. M., & Giangrande, S. E. (2020). Thermal chains and entrainment in cumulus updrafts. Part I: Theoretical description. *Journal of the Atmospheric Sciences*, 77(11), 3637–3660.
- 841
- 842
- 843 Moser, D. H., & Lasher-Trapp, S. (2017). The influence of successive thermals on entrainment and dilution in a simulated cumulus congestus. *Journal of the Atmospheric Sciences*, 74(2), 375–392.
- 844
- 845
- 846 Neggers, R., Stevens, B., & Neelin, J. D. (2006). A simple equilibrium model for shallow-cumulus-topped mixed layers. *Theoretical and Computational Fluid Dynamics*, 20(5), 305–322.
- 847
- 848
- 849 Nelson, T. C., Marquis, J., Varble, A., & Friedrich, K. (2021). Radiosonde observations of environments supporting deep moist convection initiation during RELAMPAGO-CACTI. *Monthly Weather Review*, 149(1), 289–309.
- 850
- 851
- 852 Pan, D.-M., & Randall, D. D. (1998). A cumulus parameterization with a prognostic closure. *Quarterly Journal of the Royal Meteorological Society*, 124(547), 949–981.
- 853
- 854
- 855 Peters, J. M., Hannah, W., & Morrison, H. (2019). The influence of vertical wind shear on moist thermals. *Journal of the Atmospheric Sciences*, 76(6), 1645–1659.
- 856
- 857
- 858 Peters, J. M., Morrison, H., Nelson, T. C., Marquis, J. N., Mulholland, J. P., & Nowotarski, C. J. (2022). The influence of shear on deep convection initiation. Part I: Theory. *Journal of the Atmospheric Sciences*, 79(6), 1669–1690.
- 859
- 860
- 861 Pinsky, M., Eytan, E., Koren, I., & Khain, A. (2022). Convective and turbulent motions in nonprecipitating Cu. Part II: LES simulated cloud represented by a starting plume. *Journal of the Atmospheric Sciences*, 79(3), 793–813.
- 862
- 863
- 864 Plant, R. (2010). A review of the theoretical basis for bulk mass flux convective parameterization. *Atmospheric Chemistry and Physics*, 10(8), 3529–3544.
- 865

- 866 Powell, S. W. (2022). Criticality in the shallow-to-deep transition of simulated
867 tropical marine convection. *Journal of the Atmospheric Sciences*, *79*(7), 1805–
868 1819.
- 869 Raymond, D. J., & Blyth, A. M. (1989). Precipitation development in a New
870 Mexico thunderstorm. *Quarterly Journal of the Royal Meteorological Society*,
871 *115*(490), 1397–1423.
- 872 Rio, C., Del Genio, A. D., & Hourdin, F. (2019). Ongoing breakthroughs in convective
873 parameterization. *Current Climate Change Reports*, *5*, 95–111.
- 874 Rio, C., Grandpeix, J.-Y., Hourdin, F., Guichard, F., Couvreux, F., Lafore, J.-P., ...
875 others (2013). Control of deep convection by sub-cloud lifting processes: the
876 ALP closure in the LMDZ5B general circulation model. *Climate dynamics*, *40*,
877 2271–2292.
- 878 Rio, C., Hourdin, F., Grandpeix, J.-Y., & Lafore, J.-P. (2009). Shifting the diurnal
879 cycle of parameterized deep convection over land. *Geophysical Research Letters*,
880 *36*(7).
- 881 Rochetin, N., Couvreux, F., Grandpeix, J.-Y., & Rio, C. (2014). Deep convection
882 triggering by boundary layer thermals. Part I: LES analysis and stochastic
883 triggering formulation. *Journal of the Atmospheric Sciences*, *71*(2), 496–514.
- 884 Sakradzija, M., Seifert, A., & Heus, T. (2015). Fluctuations in a quasi-stationary
885 shallow cumulus cloud ensemble. *Nonlinear Processes in Geophysics*, *22*(1),
886 65–85.
- 887 Savre, J. (2023a). Outputs from new LBA simulations. Part I: Baseline case [Data
888 set]. *Zenodo*. doi: <https://doi.org/10.5281/zenodo.10409139>
- 889 Savre, J. (2023b). Outputs from new LBA simulations. Part III: Suppressed cold
890 pools [Data set]. *Zenodo*. doi: <https://doi.org/10.5281/zenodo.10417550>
- 891 Savre, J., & Craig, G. (2023). Fitting cumulus cloud size distributions from idealized
892 cloud resolving model simulations. *Journal of Advances in Modeling Earth Sys-*
893 *tems*, *15*(5), e2022MS003360.
- 894 Savre, J., Ekman, A. M. L., & Svensson, G. (2014). Technical note: Introduction
895 to MIMICA, a large-eddy simulation solver for cloudy planetary boundary
896 layers. *Journal of Advances in Modeling Earth Systems*, *6*, 630–649. doi:
897 10.1002/2013MS000292
- 898 Schiro, K. A., & Neelin, J. D. (2019). Deep convective organization, moisture ver-
899 tical structure, and convective transition using deep-inflow mixing. *Journal of*
900 *the Atmospheric Sciences*, *76*(4), 965–987.
- 901 Schlemmer, L., & Hohenegger, C. (2014). The formation of wider and deeper clouds
902 as a result of cold-pool dynamics. *Journal of the Atmospheric Sciences*, *71*(8),
903 2842–2858.
- 904 Scorer, R., & Ludlam, F. (1953). Bubble theory of penetrative convection. *Quarterly*
905 *Journal of the Royal Meteorological Society*, *79*(339), 94–103.
- 906 Sherwood, S. C., Hernández-Deckers, D., Colin, M., & Robinson, F. (2013). Slippery
907 thermals and the cumulus entrainment paradox. *Journal of the Atmospheric*
908 *Sciences*, *70*(8), 2426–2442.
- 909 Strong, M. (2017). *Time lapse of rising cumulus congestus III – rising turrets with*
910 *pileus*. <https://www.youtube.com/watch?app=desktop&v=2rHqVFu1m6w>.
911 YouTube. (Accessed: 16.10.2023)
- 912 Suselj, K., Kurowski, M. J., & Teixeira, J. (2019). A unified eddy-diffusivity/mass-
913 flux approach for modeling atmospheric convection. *Journal of the Atmo-*
914 *spheric Sciences*, *76*(8), 2505–2537.
- 915 Takeuchi, Y. (1996). *Global dynamical properties of lotka-volterra systems*. World
916 Scientific.
- 917 Tao, C., Xie, S., Ma, H.-Y., Bechtold, P., Cui, Z., Vaillancourt, P. A., ... others
918 (2023). Diurnal cycle of precipitation over the tropics and central United
919 States: intercomparison of general circulation models. *Quarterly Journal of the*
920 *Royal Meteorological Society*. doi: 10.1002/qj.4629

- 921 Tian, Y., Zhang, Y., Klein, S. A., & Schumacher, C. (2021). Interpreting the diurnal
 922 cycle of clouds and precipitation in the ARM GoAmazon observations: Shallow
 923 to deep convection transition. *Journal of Geophysical Research: Atmospheres*,
 924 *126*(5), e2020JD033766.
- 925 Torri, G., Kuang, Z., & Tian, Y. (2015). Mechanisms for convection triggering by
 926 cold pools. *Geophysical Research Letters*, *42*(6), 1943–1950.
- 927 Vogel, R., Albright, A. L., Vial, J., George, G., Stevens, B., & Bony, S. (2022).
 928 Strong cloud–circulation coupling explains weak trade cumulus feedback. *Nature*,
 929 *612*(7941), 696–700.
- 930 Vraciu, C. V., Kruse, I. L., & Haerter, J. O. (2023). The role of passive cloud vol-
 931 umes in the transition from shallow to deep atmospheric convection. *Geophysical*
 932 *Research Letters*, *50*(23), e2023GL105996.
- 933 Wagner, T. M., & Graf, H.-F. (2010). An ensemble cumulus convection parame-
 934 terization with explicit cloud treatment. *Journal of the Atmospheric Sciences*,
 935 *67*(12), 3854–3869.
- 936 Waite, M. L., & Khouider, B. (2010). The deepening of tropical convection by
 937 congestus preconditioning. *Journal of the Atmospheric Sciences*, *67*(8), 2601–
 938 2615.
- 939 Yano, J.-I. (2014). Formulation structure of the mass-flux convection parameteriza-
 940 tion. *Dynamics of Atmospheres and Oceans*, *67*, 1–28.
- 941 Yano, J.-I., Bister, M., Fuchs, Z., Gerard, L., Phillips, V., Barkidija, S., & Piriou,
 942 J.-M. (2013). Phenomenology of convection-parameterization closure. *Atmo-*
 943 *spheric Chemistry and Physics*, *13*(8), 4111–4131.
- 944 Yano, J.-I., & Plant, R. (2012a). Finite departure from convective quasi-equilibrium:
 945 Periodic cycle and discharge–recharge mechanism. *Quarterly Journal of the*
 946 *Royal Meteorological Society*, *138*(664), 626–637.
- 947 Yano, J.-I., & Plant, R. S. (2012b). Interactions between shallow and deep convec-
 948 tion under a finite departure from convective quasi equilibrium. *Journal of the*
 949 *Atmospheric Sciences*, *69*(12), 3463–3470.
- 950 Zhao, M., & Austin, P. H. (2005). Life cycle of numerically simulated shallow cu-
 951 mulus clouds. Part II: Mixing dynamics. *Journal of the Atmospheric Sciences*,
 952 *62*(5), 1291–1310.
- 953 Zhuang, Y., Fu, R., Marengo, J. A., & Wang, H. (2017). Seasonal variation of
 954 shallow-to-deep convection transition and its link to the environmental con-
 955 ditions over the Central Amazon. *Journal of Geophysical Research: Atmo-*
 956 *spheres*, *122*(5), 2649–2666.